Transgenic mice expressing human alpha-synuclein in noradrenergic neurons develop locus coeruleus pathology and non-motor features of Parkinson's disease

Butkovich LM[1], Houser MC[1], Chalermpalanupap T[2], Porter-Stransky KA[2,3], Eidson LN[1], De Sousa Rodrigues ME[1], Oliver DL[1], Kelly SD[1], Chang J[1], Bengoa-Vergniory N[4], Wade-Martins R[4], Weinshenker D[2], Tansey MG[5]

[1] Department of Physiology, Emory School of Medicine, 30322
[2] Department of Human Genetics, Emory School of Medicine, 30322
[3] Department of Biomedical Sciences, Western Michigan University Homer Stryker M.D. School of Medicine, 49008
[4] Oxford Parkinson's Disease Centre, Department of Physiology, Anatomy and Genetics, University of Oxford, UK OX1 3QX
[5] Department of Neuroscience and Center for Translational Research in Neurodegenerative Disease, University of Florida College of Medicine, 32610

Contact:
Malú G Tansey, PhD
Department of Neuroscience
University of Florida College of Medicine
1149 Newell Drive, L5-101B
Gainesville, FL 32610
mgtansey@ufl.edu

Key words: Parkinson's disease, α-synuclein, locus coeruleus, aging, norepinephrine

Acknowledgements
This work was supported by NIH/NINDS 5F31 NS098673 (LB), NIH/NINDS F32 NS098615 (KP), NIH/NINDS 1R01 NS102306 (DW), NIH/NIA 1RF1 AG047667 (DW), NIH/NIA 1R01AG061175 (DW), NIH/NIA 1R01 AG057247 (MT), NIH/NINDS 5R01 NS092122 (MT), and NIH/NIA 3RF1 AG051514-01 (MT). This research project was supported in part by the Emory University Integrated Cellular Imaging Microscopy Core, by the Rodent Behavioral Core (RBC), which is subsidized by the Emory University School of Medicine and is one of the Emory Integrated Core Facilities. Additional support was provided by the Emory Neuroscience NINDS Core Facilities P30NS055077. Further support was provided by the Georgia Clinical & Translational Science Alliance of the National Institutes of Health under Award Number UL1TR002378. This study was supported in part by the Emory HPLC Bioanalytical Core (EHBC), which was supported by the Department of Pharmacology, Emory University School of Medicine and the Georgia Clinical & Translational Science Alliance of the National Institutes of Health under Award Number UL1TR002378. The content is solely the responsibility of the authors and does not necessarily reflect the official views of the National Institutes of Health.

Word count: Abstract =175; Introduction =603; Discussion =1471

Abstract

Degeneration of locus coeruleus (LC) neurons and dysregulation of noradrenergic signaling are ubiquitous features of Parkinson's disease (PD). The LC is among the first brain regions affected by α-synuclein (asyn) pathology, yet how asyn affects these neurons remains unclear. LC-derived norepinephrine (NE) can stimulate neuroprotective mechanisms and modulate immune cells, while dysregulation of NE neurotransmission may exacerbate disease progression, particularly non-motor symptoms, and contribute to the chronic neuroinflammation associated with PD pathology. Although transgenic mice overexpressing asyn have previously been developed, transgene expression is usually driven by pan-neuronal promoters and thus has not been selectively targeted to LC neurons. Here we report a novel transgenic mouse expressing human wild-type asyn under control of the noradrenergic-specific dopamine β-hydroxylase promoter. These mice developed asyn aggregates in LC neurons, alterations in hippocampal and LC microglial abundance, upregulated GFAP expression, degeneration of LC fibers, decreased striatal dopamine metabolism, and age-dependent behaviors reminiscent of non-motor symptoms of PD. These mice provide novel insights into how asyn pathology affects LC neurons and how LC dysfunction may contribute to early PD pathophysiology.

Significance statement

α-synuclein (asyn) pathology and loss of neurons in the locus coeruleus (LC) are two of the most ubiquitous neuropathologic features of Parkinson's disease (PD). Dysregulated NE neurotransmission is associated with the non-motor symptoms of PD including sleep disturbance, emotional changes such as anxiety and depression, and cognitive decline. Importantly, loss of central NE may contribute to the chronic inflammation in, and

70 progression of, PD. We have generated a novel transgenic mouse expressing human
71 wild-type asyn in LC neurons to investigate how increased asyn expression affects the
72 function of the central noradrenergic transmission and associated behaviors. We report
73 cytotoxic effects of asyn overexpression associated with astrogliosis in the LC and LC
74 target regions, degeneration of LC fibers with disruptions in striatal dopamine (DA)
75 metabolism, and age-dependent alterations in non-motor behaviors.

76 **Introduction**

77 Brain regions affected in Parkinson's disease (PD) exhibit proteinaceous aggregates
78 (known as Lewy bodies) primarily composed of α-synuclein (asyn), chronic inflammation,
79 and neuron loss (den Hartog and Bethlem, 1960; Spillantini et al., 1997; Tansey and
80 Goldberg, 2010). Striatal dopamine (DA) and DA transporter (DAT) are deficient in PD,
81 but other neurotransmitter systems are affected including acetylcholine, serotonin, and
82 norepinephrine (NE) (Gonera et al., 1997; Abbott et al., 2005; Ross et al., 2008).
83 The locus coeruleus (LC) is among the first brain regions affected in PD. The LC is a
84 bilateral pontine nucleus at the lateral floor of the fourth ventricle, and is the main source
85 of NE for the central nervous system (CNS) (Iversen et al., 1983; Mann et al., 1983; Braak
86 et al., 2001). Asyn aggregates and neuronal degeneration in the LC are ubiquitous
87 features of PD and are associated with non-motor symptoms including sleep disorders,
88 mood disturbances, and cognitive deficits (Iversen et al., 1983; Chui et al., 1986; German
89 et al., 1992; Braak et al., 2001; Zarow et al., 2003; Weinshenker, 2018). Imaging and
90 histological studies show a progressive loss of central NE, noradrenergic neurons, and
91 accumulation of asyn pathology in the LC in PD (Halliday et al., 1990; German et al.,
92 1992; Brunnstrom et al., 2011; Pifl et al., 2012; Keren et al., 2015) which may exacerbate

93 degeneration of DA neurons in the midbrain substantia nigra pars compacta (SNpc)
94 (Zarow et al., 2003; Chen et al., 2014).
95 Depletion of LC-NE exacerbates 6-hydroxydopamine (6-OHDA) or 1-methyl-4phenyl-
96 1,2,3,6-tetrahydropyridine (MPTP)-induced nigrostriatal pathology in rodents and
97 primates (Mavridis et al., 1991; Srinivasan and Schmidt, 2003; Rommelfanger et al.,
98 2007), while increasing extracellular NE is protective (Kilbourn et al., 1998;
99 Rommelfanger et al., 2004; Kreiner et al., 2019). Furthermore, lesioning LC neurons
100 induces inflammation, and dysregulated NE neurotransmission may contribute to the
101 chronic inflammation seen in PD (Kim and Joh, 2006; Tansey and Goldberg, 2010; Yao
102 et al., 2015; Bharani et al., 2017; Song et al., 2018).
103 The initiating event in asyn aggregation in sporadic PD is unclear, but a candidate
104 mechanisms include environmental exposures, and increased expression of asyn, as
105 individuals with a multiplication mutation in the gene encoding asyn (*SNCA*) develop
106 autosomal dominantly-inherited PD (Singleton et al., 2003; Chartier-Harlin et al., 2004;
107 Ferese et al., 2015). Age is the primary risk factor for PD, and rodent models of asyn
108 overexpression develop age-dependent asyn aggregates and PD-like behavioral
109 abnormalities (Masliah et al., 2000; Giasson et al., 2002; Hansen et al., 2013). However,
110 in most of these models, transgene expression is driven by a pan-neuronal promoter with
111 asyn overexpression in multiple regions of the CNS, with only one model reporting LC
112 pathology (Masliah et al., 2000; Giasson et al., 2002; Maskri et al., 2004; Schell et al.,
113 2009; Koprich et al., 2010; Sotiriou et al., 2010; Delenclos et al., 2017). Viral-mediated
114 expression has been used to target asyn overexpression to specific brain regions
115 (Baekelandt et al., 2002; Kirik et al., 2002; Delenclos et al., 2017; Ip et al., 2017; Niu et

al., 2018). Notably, viral overexpression of a familial PD mutant asyn in LC neurons resulted in asyn aggregation, inflammation, and degeneration of LC neurons (Henrich et al., 2018). To investigate specifically how pathology induced by wild-type asyn affects noradrenergic neurons in the LC in an aging organism, we targeted expression of human wild-type asyn to LC neurons under control of the noradrenergic/adrenergic-specific dopamine β-hydroxylase (DBH) promoter using bacterial artificial chromosome (BAC) transgenesis. To determine the molecular, cellular, and behavioral age-dependent consequences of increased asyn expression in LC neurons, 3-, 14-, and 24-month (mo) old DBH-hSNCA transgenic (Tg) mice and non-transgenic (nTg) littermate controls were examined.

Methods

Experimental design. To determine how expression of human asyn in LC neurons affects neuronal health and LC-NE-associated behaviors, mice were aged undisturbed until the time of behavioral testing or sacrifice at ages 3-, 14-, and 24-mos.

Generation of the DBH-hSNCA mouse model. Male and female mice expressing human wild-type α-synuclein (DBH-hSNCA) were engineered using a commercially available human bacterial artificial chromosomal (BAC) RP11-746P3 (Cubells et al., 2016) encompassing the *DBH* gene. The wild-type *hSNCA* cDNA open reading frame (400bp) was targeted to the translational start site of *DBH* by standard BAC recombineering methods by the University of North Carolina – Chapel Hill Molecular Neuroscience Core (currently Animal Model Core). The BAC construct was injected into C57BL/6N pronuclei by the Emory University Mouse Transgenic and Gene Targeting Core Facility (http://www.cores.emory.edu/tmc/index.html), transgene expression in

139 founder pups was determined by PCR, and breeding lines were established. Mice
140 carrying the hSNCA sequence were crossed with wild-type C57Bl/6N mice (Charles
141 River) to establish the hemizygous transgenic DBH-hSNCA line.
142 To improve efficiency and accuracy of LC tissue isolation for western blot and mRNA
143 analysis, DBH-hSNCA mice were crossed with the TH-EGFP reporter mouse expressing
144 enhanced green fluorescent protein (EGFP) under the tyrosine hydroxylase (TH)
145 promotor (Sawamoto et al., 2001).
146 **Animals.** Male and female DBH-hSNCA mice were maintained on a C57Bl/6 background.
147 Mice were group housed (maximum 5 mice per cage) until two weeks prior to the start of
148 behavioral testing, when they were singly housed until euthanized. Animals were
149 maintained on a 12/12h light/dark cycle with access to standard rodent chow and water
150 *ad libitum*. Hemizygous animals served as experimental mice, with non-transgenic
151 littermates as controls. Genotypes were determined by tail snip PCR with two sets of
152 primers: Forward 5' TGTCCAAGATGGACCAGACTC 3' Reverse 3'
153 ACTGGTCTGAGGCAGGGAGCA 5'; Set Forward 5' GCCCTCAGTCTACTTGCGGGA 3'
154 Reverse 3' GCGAGAGCATCATAGGGAGT 5'. Experimental procedures involving use of
155 animals were performed in accordance with the NIH Guidelines for Animal Care and Use
156 and approved by the Institutional Animal Care and Use Committee at Emory University
157 School of Medicine.
158 **Sleep latency test.** Latency to fall asleep was quantified as the duration of time following
159 gentle handling until their first sleep bout, which was defined as sleeping continuously for
160 2 min, and for a total of 75% of the 10-min period that began at sleep onset (Hunsley and
161 Palmiter, 2004). Sleep testing began at 9 AM, 2 h into the light cycle when internal

162 pressure to sleep is high. The sessions were video recorded and scored by
163 an experienced observer blind to the genotype. We have validated this behavioral sleep
164 scoring method with EEG (Porter-Stransky et al., 2019).
165 **Marble burying test.** Marble burying was conducted as previously described (de Sousa
166 Rodrigues et al., 2017) to determine whether expression of human asyn in LC neurons
167 promotes anxiety-like behavior. Mice were placed in a plastic tub (50.5 x 39.4 x 19.7 cm)
168 containing 5 inches of lightly pressed bedding. Twenty marbles of uniform size and color
169 were placed in 5 rows of 4 marbles each on top of the bedding. Mice were placed in the
170 containers and allowed to roam freely for 30 min. At the end of testing, the mice were
171 placed back in home cages, and the number of marbles buried at least two-thirds of their
172 height were counted. Marble burying was conducted 2 weeks after sleep latency testing.
173 **Open Field testing.** In the open field test, a mouse that spends less time in or hesitates
174 to re-enter the open center of the testing chamber is considered to be exhibiting anxiety-
175 like behavior (Britton and Britton, 1981). During the light phase of the light/dark cycle,
176 mice were acclimated to a dark testing room under red light for 1 h before testing. Mice
177 were placed into the open field (45 cm X 45 cm square box) and allowed to move freely
178 for 10 min. Distance, velocity, center, and border statistics were measured using
179 Noldus/Ethovision software. Center was defined as the central 22.5 cm X 22.5 cm. Open
180 field was conducted 1 week after marble burying.
181 **Circadian locomotion.** All testing mice were acclimated to the testing room for 2 d prior
182 to the experiment. Mice were each placed in a clear Plexiglas (15.75” L, 13.25” L, 7.38”
183 H) activity cage equipped with infrared photobeams (San Diego Instruments, La Jolla,
184 CA). Food and water were available *ad libitum* during the 23-h testing period. Ambulations

185 (consecutive photobeam breaks) were recorded by PAS software. Circadian locomotion
186 behavior was assessed 2 weeks after open field testing.
187 **Fear conditioning.** Fear conditioning training and contextual and cued fear testing is a
188 test of memory for the association of an aversive stimulus with an environment cue or
189 context, and was conducted as previously described (Chalermpalanupap et al., 2018)
190 over 3 consecutive days. Mice were placed in the fear conditioning apparatus (7" W, 7"
191 D, 12" H, Coulbourn) with metal shock grid floor and allowed to explore the enclosure for
192 3 min. Following habituation, three conditioned stimulus (CS)-unconditioned stimulus
193 (US) pairings were presented with a one-min inter-trial interval. The CS was a 20 sec 85
194 db tone, and the US was a 2 sec 0.5mA footshock (Precision Animal Shocker, Colbourn)
195 which co-terminated with CS presentation. The contextual test was conducted on the
196 following day when animals were placed back into the same chamber. On day three, the
197 animals were placed in a novel compartment and allowed to habituate for 2 min. Following
198 habituation, the 85 db tone was presented, and the amount of freezing behavior recorded.
199 No shocks were given during the contextual or cued tests. Fear conditioning was
200 conducted 1 week after circadian locomotion behavior.
201 **Tissue collection.** Animals used in immunohistochemical and high-performance liquid
202 chromatography (HPLC) analyses were anesthetized by injection of sodium pentobarbital
203 (Euthasol, Virbac) until unresponsive. Mice were transcardially perfused with phosphate-
204 buffered saline (PBS; pH 7.4) until exiting blood ran clear. Brain tissue was removed, with
205 one hemisphere post-fixed in 4% paraformaldehyde for immunohistochemistry, and the
206 other dissected and flash frozen for HPLC. Animals used for qPCR or western blot

207 analyses were euthanized by cervical dislocation under isoflurane anesthesia. Tissue was
208 flash frozen and stored at -80°C until processing.
209 **Immunohistochemistry.** Brain tissue was sectioned on a freezing microtome (Leica
210 SM2010R, Buffalo Grove, IL) at 40µm and stored in cryoprotectant (30% ethylene glycol,
211 30% sucrose, 13.32mM NaH_2PO_4, 38.74mM Na_2HPO_4, 250µM Polyvinylpyrrolidone)
212 solution at -20°C until staining. Sections were washed in PBS before blocking in 5%
213 normal goat serum (Jackson ImmunoResearch 005-000-121; NGS) with 0.05% Triton X-
214 100 (Sigma #T9284100) in Tris-buffered saline pH 7.4 (TBS) for 1 h at room temperature.
215 Sections were transferred directly to primary antibody solution containing 1% NGS, 0.05%
216 Triton-X 100, and antibody at the concentrations described in Table 1 and incubated
217 overnight at room temperature (05-02 Ms anti-NET, 1:1,000) or 4°C (all other primary
218 antibodies). Fluorescently conjugated secondary antibodies (described in Table 1) were
219 diluted in 0.1% NGS with 0.05% Triton X-100, and tissue sections were incubated for 1 h
220 at room temperature in the dark. Sections were mounted on Superfrost Plus slides (VWR)
221 and were coverslipped with Vectashield with DAPI (Vector). All immunofluorescent
222 images were acquired as z-stack images and the file compressed on a Keyence BZ-X700
223 microscope system (Itasca, IL). The Allen Brain Atlas version 1 (2008) was used to
224 identify regions of interest (ROIs). One section per mouse containing the dorsal
225 hippocampus (near bregma -1.995 mm) and one containing the LC (bregma -5.555 mm)
226 were analyzed for percent immunoreactivity (IR) within a standard ROI. A detection
227 threshold was set uniformly across images in each analysis, and % IR determined using
228 the “Measure” feature of ImageJ. Percent IR was calculated as area of IR within the ROI
229 divided by the total ROI area and multiplied by 100. Quantification of Iba1-positive cells

230 (microglia) was also analyzed with a standard threshold, ROI, and upper and lower size
231 limits (pixel^2) using the “Analyze particles” function in ImageJ.

232 **Proximity ligation assay (PLA).** Paraffin embedded tissue was rehydrated by
233 consecutive incubations in Xylene, Histoclear, 100% ethanol, 95% ethanol, 70% ethanol
234 and H_2O. Samples were then incubated in 10% H_2O_2 in PBS to reduce background and
235 heated in a microwave in citrate buffer (pH 6.0; Abcam) for antigen retrieval. After antigen
236 retrieval, samples were processed for immunofluorescence: 1 h RT incubation in 10%
237 Serum with 0.05% Tween-20 in TBS block, 1 h incubation in primary antibody, TBS with
238 0.05% Tween-20 (TBS-T) wash. Slides were then incubated for 1 h with secondary
239 antibodies (Alexa488 Life Technologies), and washed again with TBS-T. For
240 immunohistochemistry, samples were then coverslipped with FluorSave (Calbiochem).
241 For PLA, samples were covered in manufacturers PLA blocking solution (Sigma) for 1 h
242 at 37°C, and then incubated overnight with PLA conjugates (a-syn211; ab80627 Abcam).
243 On the next day, samples were washed with TBS-T, incubated in ligation solution for 1 h
244 at 37C°, washed with TBS-T, incubated in amplification solution for 2.5 h at 37C°, washed
245 with TBS, counterstained with DAPI, and mounted with FluorSave. All PLA reagents were
246 used as per manufacturer’s instructions (Sigma; cat #92008).
247 PLA puncta were counted blindly from 25 cells per LC section per animal. Two
248 independent experimental rounds were normalized and averaged in order to provide the
249 final quantification.
250

251 **RNA Scope.** *In situ* RNA analysis was performed using RNAScope Multiplex Fluorescent
252 v2 kit (ACD Bio 3231000). Tissue prep and analysis were conducted as described in
253 manufacturer’s protocol. Briefly, following transcardial perfusion with saline, brains were
254 incubated in 4% paraformaldehyde (PFA) for 24 hours followed by a series of increasing
255 sucrose concentrations before being frozen in optimal temperature cutting medium
256 (Sakura) and stored at -80°C until sectioning. Tissue sections (12μm) were collected on

257 a Leica CM1900 cryostat and mounted on Superfrost Plus slides. To prevent tissue
258 detachment, slides were dried at 60°C for 30 min and fixed in 4% PFA for 15 min at 4°C
259 before ethanol dehydration. Tissue was processed as described in ACD Bio protocol
260 (acdbio.com/technical-support/user-manuals #323100-USM).
261
262 **Western immunoblotting.** Western blots were conducted as previously described (de
263 Sousa Rodrigues et al., 2017). Flash frozen samples were stored at -80°C until
264 processing. Protein was isolated from LC samples with RIPA buffer (1% Triton-X 100,
265 50mM Tris HCL, 0.1% sodium dodecyl sulfate, 150mM NaCL, pH 8.0), or Trizol (Life
266 Technologies #15596-018). RIPA samples were centrifuged at 12,000 rpm for 20 min at
267 4°C. Supernatant was transferred to new tube for bicinchoninic acid protein assay (Pierce
268 Scientific #23225). Trizol samples were resuspended in 1% SDS. Samples were diluted
269 to 1µg/µl in 4x sample buffer (BioRad #1610747) and boiled at 90°C for 5 min.
270 Electrophoresis was performed using 12% gels (BioRad #4568046; 5µl) and transferred
271 to 0.45µm PVDF membrane using Trans-Blot Turbo Transfer System (BioRad). For asyn
272 immunoblotting, the membrane was fixed in 0.4% PFA for 30 min following transfer. After
273 a brief wash, blots were incubated in 5% milk blocking buffer (BioRad) for 1 hour at 4°C
274 before primary antibody overnight at 4°C. Membranes were washed with TBST (0.01%
275 Tween-20) and incubated in HRP-conjugated secondary antibodies in blocking buffer for
276 1 hour at room temperature. Images were acquired using Azure Biosystems and analyzed
277 by ImageStudio Lite software. Protein expression was normalized to total protein (Li-Cor
278 #926-11015).
279 **High performance liquid chromatography (HPLC).**

280 Monoamines were examined by high performance liquid chromatography with
281 electrochemical detection as described previously (Song et al., 2012). For HPLC, an ESA
282 5600A CoulArray detection system, equipped with an ESA Model 584 pump and an ESA
283 542 refrigerated autosampler was used. Separations were performed using an MD-150 ×
284 3.2 mm C18 (3 μM) column at 25ºC. The mobile phase consisted of 8% acetonitrile, 75
285 mM NaH_2PO4, 1.7 mM 1-octanesulfonic acid sodium and 0.025% trimethylamine at pH
286 2.9. Twenty-five microliters of sample were injected. The samples were eluted
287 isocratically at 0.4 mL/min and detected using a 6210-electrochemical cell (ESA, Bedford,
288 MA) equipped with 5020 guard cell. Guard cell potential was set at 475 mV, while
289 analytical cell potentials were −175, 150, 350 and 425 mV. The analytes were identified
290 by the matching criteria of retention time and sensor ratio measures to known standards
291 (Sigma Chemical Co., St. Louis MO.) consisting of dopamine, norepinephrine, 3,4-
292 dihydroxyphenylacetic acid (DOPAC), and 4-Hydroxy-3-methoxyphenylglycol (MHPG).
293 Compounds were quantified by comparing peak areas to those of standards on the
294 dominant sensor.
295 **Statistical analysis.** Student's t-test was used to assess differences by genotype within
296 each age group in sleep latency, marble burying, open field, western blot, and all
297 immunofluorescent analyses. Repeated measures two-way ANOVA was used to analyze
298 differences by genotype within each age group in fear conditioning, and circadian
299 locomotor assay followed by Tukey's post hoc test where applicable. Comparisons across
300 age groups were not conducted, as behavioral assays, HPLC, and immunofluorescence
301 of each cohort were conducted at separate time points. The analyses were performed

302 using GraphPad Prism 7 (GraphPad Software, Inc., La Jolla, CA) with a p-value threshold
303 of <0.05.

304 **Results**

305 **Generation of DBH-hSNCA mice**

306 The DBH-hSNCA mouse model was developed using a DBH-BAC construct carrying the
307 wild type human *SNCA* cDNA open reading frame at the translational start site of *DBH*
308 (Fig. 1). Transgene integration was confirmed by PCR, and founder mice were bred with
309 wild type C57BL/6 mice to establish the hemizygous DBH-hSNCA line.

310 **Human *Snca* mRNA is expressed in DBH-hSNCA LC neurons**

311 Fluorescent *in situ* mRNA analysis revealed human *Snca* mRNA in Tg LC neurons (Fig
312 2), which co-localized with mouse *Th* and mouse *Dbh* mRNA, while human *Snca* mRNA
313 expression was not detected in nTg LC neurons.

314 **Human asyn is expressed in LC neurons of DBH-hSNCA transgenic mice**

315 Human asyn protein was analyzed by immunofluorescence and western blot. Using an
316 antibody specific for human asyn (Biolegend 807801), expression of human asyn was
317 found to co-localize with TH-expressing LC neurons only in brain sections from DBH-
318 hSNCA Tg mice (Fig. 3A). No human asyn-specific immunofluorescence was detected
319 in LC neurons of nTg littermates or in SNpc neurons regardless of genotype (Fig. 3A,C).
320 Human asyn was also detectable specifically in LC protein lysate from Tg tissue by
321 immunoblot and not in nTg lysates (Fig 3B; n=4). Quantitative western blot analysis of LC
322 protein using a pan-asyn antibody to detect both human and mouse asyn protein revealed
323 a significant ~30% increase of total asyn in Tg mice at 3-mo relative to that in nTg

324 littermates (Fig 3D; $t_{(6)}$=3.156, p=0.0197, n=4). Human *SNCA* mRNA expression in Tg LC
325 neurons was confirmed by qPCR (Data not shown).

326 **DBH-hSNCA mice exhibit behavioral phenotypes that resemble features of non-**
327 **motor PD symptoms**

328 A primary role of the LC-NE system is promoting arousal and wakefulness; LC activity is
329 highest just prior to, and during wake (Hobson et al., 1975). Sleep disturbances are one
330 of the most common non-motor PD symptoms, and PD patients with disturbed sleep have
331 greater asyn pathology in the LC than PD patients without sleep complaints (Kalaitzakis
332 et al., 2013). Thus, sleep latency was assessed to examine whether features of the
333 sleep/wake cycle were affected by human asyn expression in the LC. Mice were gently
334 handled and returned to their home cage, and video recording was scored by an observer
335 blind to the genotype to determine latency to fall asleep. Our findings indicate that there
336 was a significant increase in sleep latency in Tg mice at 3-mos, (Fig 4A; $t_{(14)}$=4.36
337 p=0.0007; n=8) and 14-mos ($t_{(17)}$=2.51, p=0.0225; n=9), indicative of an elevated arousal
338 state. No differences were observed at 24-mos ($t_{(8)}$=0.821, p=0.4354, n=7-8).

339 LC neurons are activated by stress exposure, and blocking LC activity abolishes stress-
340 induced anxiety-like behavior (McCall et al., 2015). In PD, anxiety severity is inversely
341 correlated with LC function (Remy et al., 2005). To examine anxiety-like behavior, the
342 behavior DBH-hSNCA mice was assessed in marble burying and open field tests. In the
343 marble burying assay, there was a significant increase in the number of marbles buried
344 by Tg mice at 14- (Fig 4B; $t_{(18)}$=2.735, p=0.0136; n=8-12) and 24-mos ($t_{(13)}$=2.212,
345 p=0.0455, n=7-8). In open field tests, an age-dependent anxiety-like phenotype was also
346 evident in 14-mo Tg mice, evinced by an increase in the latency to re-enter the center of

347 the testing field (Fig 4C; $t_{(17)}$2.359, p=0.0305; n=7-12), with no differences in 3-
348 ($t_{(11)}$=0.1988, p=0.8460, n=7-8) or 24-mo old animals ($t_{(11)}$=0.5075, p=0.6219, n=7-8).
349 Fear conditioning is a measure of hippocampal-dependent (contextual) or -independent
350 (cued) associative learning (Phillips and LeDoux, 1992), and mice lacking NE exhibit
351 impaired contextual learning (Murchison et al., 2004). In a standard fear conditioning
352 paradigm, 14-mo old DBH-hSNCA Tg mice exhibited increased freezing behavior during
353 the fear training session (Fig 4D center; Interaction $F_{(6, 120)}$=2.735, p=0.0159; n=8-14), as
354 well as during the contextual test (Fig 4E center; effect of genotype $F_{(1, 20)}$=5.566,
355 p=0.0286), with no differences in freezing behavior during the cued test (Fig 4F). No
356 genotype differences were found in the fear training (Fig 4D), contextual test (Fig 4E), or
357 cued test (Fig 4F) in 3- or 24-mo old mice.
358 Because disruption in locomotor activity can affect behavioral testing, we evaluated the
359 locomotion over 24 h and found no genotype differences at 3- ($F_{(1, 12)}$=1.158, p=0.3031;
360 n=7), 14- ($F_{(1, 11)}$=0.1864, p=0.6743; n=7), or 24-mos ($F_{(1, 13)}$=0.0603, p=0.8099; n=7-8) of
361 age (Fig. 4F). Initially, all groups had high levels of activity, as would be expected in a
362 novel environment, which decreased as mice habituated to the test apparatus.
363 Ambulations increased normally in all genotypes at commencement of the dark phase,
364 when mice are typically more active, and decreased once the next light cycle began.
365 However, the 14-mo old Tg mice exhibited significantly more rearing behavior during the
366 dark phase than the nTg mice (Fig 4G; Interaction $F_{(21, 231)}$=1.911, p=0.0113).
367

368 **Human asyn forms aggregates in LC neurons at 14-mos of age**

369 To determine whether transgenic expression of human asyn in LC neurons leads to
370 formation of asyn aggregates, tissue sections containing the LC were analyzed using a
371 human asyn proximity ligation assay (PLA). In 14-mo old Tg mice (Fig 5), LC neurons
372 displayed more asyn puncta per field than LC neurons from nTg mice ($t_{(8)}$=2.532,
373 p=0.0352; n=4-6). Asyn aggregates are fibril-rich and highly phosphorylated at residue
374 129 (pSer129), and labeling these forms of the protein is commonly used to identify asyn
375 aggregates (Fujiwara et al., 2002; Wakamatsu et al., 2007; Schell et al., 2009). Therefore,
376 we immunolabeled tissue sections with an antibody specific for fibril-rich asyn (Syn-F1)
377 or asyn pSer129 and found no detectable signal (data not shown), suggesting that at 14
378 mos of age the asyn-immunoreactive puncta are likely to represent intermediate asyn
379 oligomers rather than mature aggregates.
380
381 **Human asyn expression in LC neurons impacts striatal dopamine metabolism in**
382 **24-mo old mice**
383 Dysregulated catecholamine metabolism and degeneration of catecholaminergic neurons
384 are well-established features of PD (Iversen et al., 1983; Mann et al., 1983; Hirsch et al.,
385 1988; Fearnley and Lees, 1991). Therefore, we measured catecholamine levels using
386 high-performance liquid chromatography (HPLC). Hippocampal and striatal tissue
387 content of NE, the NE metabolite MHPG, DA, and the DA metabolite DOPAC were
388 quantified, revealing that NE (Fig. 6A,B) and DA (Fig. 6E,F) were not significantly affected
389 in the hippocampus or striatum at any age Similarly, the ratio of the major NE metabolite
390 MHPG to NE was unaffected (Fig, 6C,D). The ratio of the DA metabolite DOPAC to DA
391 in the hippocampus was unaltered (Fig. 6G), but was significantly reduced in the Tg

392 striatum at 24-mos (Fig 6H; $t_{(10)}$=3.546, p=0.0046; n=5-7), consistent with decreased DA
393 turnover.
394
395 **Human asyn expression does not affect LC neuronal integrity**
396 LC neurons were visualized using NET immunoreactivity (IR). NET is a reliable marker of
397 LC neurons, and its expression is reduced in PD patients (Remy et al., 2005). Using a
398 standard ROI, no difference in the percent NET IR was detected between genotypes at
399 3- (Fig 7; $t_{(17)}$=0.4537, p=0.6558; n=9-10), 14- ($t_{(10)}$=0.8908, p=0.3939; n=5-7), or 24-mos
400 ($t_{(8)}$=0.8069, p=0.4430; n=5-7).
401 **Elevation of tyrosine hydroxylase in the LC of DBH-hSNCA mice**
402 Tyrosine hydroxylase (TH) is the rate-limiting enzyme in NE and DA synthesis, and its
403 long-term activity depends on its expression levels (Levitt et al., 1965; Haycock, 1993;
404 Kumer and Vrana, 1996). To determine whether TH expression in the LC is affected by
405 human asyn, we assessed TH IR in sections from 3-, 14-, and 24-mo old mice. TH IR was
406 normalized to NET IR to control for potential differences in Bregma level between
407 sections. TH expression was increased in Tg LC neurons (Fig 8A,B) at both 3-
408 ($t_{(17)}$=2.154, p=0.0459; n=9) and 14-mo ($t_{(10)}$=2.463, p=0.0335; n=5-7) of age. Western
409 blot analysis from 3-mo old TH-EGFP-expressing LC neurons (Fig 8C,D) confirmed
410 higher TH expression in Tg animals ($t_{(10)}$=3.837, p=0.0033; n= 5-7).
411 **Human asyn expression in LC neurons affects expression of local inflammatory**
412 **markers**
413 A wealth of studies suggest that dysregulated noradrenergic neurotransmission is
414 associated with inflammation (reviewed by Butkovich et al. 2018), and that dysregulation

415 of the LC-NE system could contribute to the chronic neuroinflammation observed in PD
416 (Fujita et al., 1998; Gyoneva and Traynelis, 2013; Johnson et al., 2013; Butkovich et al.,
417 2018). To determine whether human asyn expression in LC neurons affects the number
418 of myeloid cells in the brain (both brain-resident microglia and potentially infiltrating
419 monocytes), we quantified the number of Iba1-positive cells in the LC by
420 immunofluorescence. At 14-mo, there was a significant decrease in the number of Iba1-
421 expressing cells in the LC of Tg animals (Fig 9A,B; $t_{(13)}$=2.845, p=0.0138; n=8), with no
422 changes at other ages. To determine astrocyte activation, we quantified glial fibrillary
423 acidic protein (GFAP) IR, commonly used as a protein marker of astrogliosis (Eng and
424 Ghirnikar, 1994), in the LC. At 24-mo, there was a significant increase in astrocytic GFAP
425 expression in the LC of Tg animals (Fig 9C, D; $t_{(10)}$=2.744, p=0.0207; n=5-7).

426 **Human asyn expression in LC neurons is associated with loss of hippocampal LC**
427 **fibers at 24-mos**

428 The LC is the sole source of hippocampal NE, which is necessary for proper memory
429 formation and retrieval (Devauges and Sara, 1991). Noradrenergic LC fibers express
430 NET, and PD brain tissue shows substantial LC denervation (Pavese et al., 2011). To
431 determine whether hippocampal LC projections degenerate in DBH-hSNCA mice, we
432 examined NET IR in the CA1, CA3, and dentate gyrus regions of the hippocampus. At
433 24-mos, we found a reduction in LC fibers in the dentate gyrus (Fig 12C,D; $t_{(10)}$=2.974,
434 p=0.0156; n=5-7), with a trend for reduction in CA1 (Fig 12A, B; $t_{(10)}$=1.899, p=0.0901)
435 and CA3 (Fig 12E,F; $t_{(10)}$=1.538, p=0.1585). No differences were observed in mice at 3-,
436 or 14-mos.

437

438 **Hippocampal astrogliosis and changes in number of hippocampal Iba1-expressing**
439 **cells in aged DBH-hSNCA mice**

440 To determine whether degeneration of hippocampal LC projections is associated with
441 inflammation, GFAP IR was visualized in the CA1, CA3, and dentate gyrus regions of the
442 hippocampus. At 14-mos, there was a significant increase in GFAP expression in CA1
443 (Fig 10A,B; $t_{(19)}$=2.723 ,p=0.0135, n=9-12) and CA3 (Fig 10E,F; $t_{(19)}$=2.275 ,p=0.0347),
444 but not the dentate gyrus (Fig 11C,D; $t_{(19)}$=1.607, p=0.1246), of Tg mice. Similar to what
445 we observed in the LC, the number of Iba1-expressing cells in CA1 was reduced in Tg
446 mice at 14-mos (Fig 11; $t_{(16)}$=2.592, p=0.0196, n=9).

447

448 **Discussion**

449 Based on a wealth of evidence (Mavridis et al., 1991; Srinivasan and Schmidt, 2003; Tong
450 et al., 2006; Rommelfanger et al., 2007; Yao et al., 2015), we posit that asyn pathology
451 and degeneration of LC neurons may represent a tipping point in PD progression;
452 therefore, understanding how asyn accumulation in LC neurons affects their function and
453 survival may help inform development of new therapeutics for earlier interventions. To
454 this end, we developed a new BAC transgenic mouse expressing human wild-type asyn
455 under the control of the noradrenergic-specific DBH.

456 Human asyn was detectable in Tg LC neurons by immunofluorescence and western blot
457 at 3-mos. Analysis of total asyn (mouse + human) revealed that the total asyn burden is
458 increased in Tg LC neurons at 3-mos. While pSer129-positive, or fibrillar asyn aggregates
459 were not detected in LC neurons at any age, increasing the burden of asyn expression in
460 LC neurons resulted in the formation of putative oligomeric asyn aggregates. In PD, asyn

461 aggregates appear prior to neuron degeneration (Chevalier-Larsen and Holzbaur, 2006;
462 Chu et al., 2012), and while we observed no loss of LC cell bodies, NET-expressing fibers
463 were reduced in the hippocampus of 24-mo old mice. This finding resembles the pattern
464 of neuron death observed in PD, with axon terminals degenerating prior to frank cell loss
465 in the LC (Hornykiewicz, 1998). Interestingly, the selective loss of LC fibers in the dentate
466 gyrus of DBH-hSNCA mice is reminiscent of what we observed in TgF344-AD rat model
467 of Alzheimer's disease that accumulates tau pathology in the LC (Rorabaugh et al., 2017).
468 To determine the functional outcome of asyn aggregates in LC neurons, we measured
469 catecholamine levels in the hippocampus and striatum. Despite the loss of hippocampal
470 LC fibers at 24-mos we did not detect changes in hippocampal NE content by HPLC,
471 which may indicate a compensatory enhancement in NE neurotransmission. We
472 observed a trend toward decreased striatal NE 24-mos, although it was not statistically
473 significant. The sparse innervation by NE, it is possible that changes in NE
474 neurotransmission are detectable in the striatum prior to more densely innervated
475 regions. Dysregulated DA metabolism is a central feature of PD (Leenders et al., 1990),
476 and midbrain dopaminergic innervation to the striatum is modulated by LC-NE (Lategan
477 et al., 1990; Grenhoff et al., 1993; Rommelfanger et al., 2007; Rommelfanger and
478 Weinshenker, 2007). Studies of catecholamine function in rodents show that enhancing
479 LC-NE stimulates midbrain DA release in the striatum, whereas LC lesions or NE
480 deficiency reduce striatal DA release (Lategan et al., 1990; Grenhoff et al., 1993; Schank
481 et al., 2006). We found that at 24-mos, Tg mice had a reduced striatal ratio of DOPAC:DA,
482 and a trend toward increased DA, suggesting that human asyn expression in aging LC
483 neurons causes a reduction in striatal DA turnover. Future studies will determine whether

484 NE innervation to midbrain DA neurons is reduced in 24-mo DBH-hSNCA mice, and
485 whether loss of noradrenergic transmission impairs striatal DA release. While no
486 significant differences were detected in hippocampal or striatal NE content at any age, Tg
487 LC neurons had increased TH expression at 3- and 14-mos relative to nTg littermates,
488 suggesting an increased capacity for NE synthesis.
489 Neuroinflammation is a central feature of PD pathology (McGeer et al., 1988; Gerhard et
490 al., 2006; Tansey and Goldberg, 2010), with extensive evidence of changes in microglial
491 activation in brain regions that degenerate in PD (Kim and Joh, 2006; Tansey and
492 Goldberg, 2010), and we know that microglia and astrocyte functions are modulated by
493 NE neurotransmission (Fahrig, 1993; Heneka et al., 2010; Bharani et al., 2017).
494 Unexpectedly, we observed fewer Iba1-expressing cells in the LC and CA1 region of the
495 hippocampus of DBH-hSNCA mice at 14-mos compared to nTg littermates. It has been
496 reported that NE can modulate microglial activity, and the functional outcome of microglia
497 adrenergic receptor activation appears to depend on the physiological context (Fujita et
498 al., 1998; Gyoneva and Traynelis, 2013; Johnson et al., 2013). At 14-mos, there was an
499 increase in hippocampal astrocytic GFAP expression. Astrocytes throughout the brain are
500 activated by NE, and ARs signal transduction stimulates transient calcium release, and
501 release of inflammatory signaling molecules by astrocytes (Norris and Benveniste, 1993;
502 Duffy and MacVicar, 1995; Paukert et al., 2014). However, the number GFAP-expressing
503 astrocytes is inversely correlated to the amount of dopaminergic cell loss in PD and
504 increased GFAP immunoreactivity in the hippocampus occurred prior to loss of LC
505 projections (Damier et al., 1993; Eng and Ghirnikar, 1994). Further studies are required
506 to determine whether increased GFAP activity is due to dysregulated NE

507 neurotransmission, or an inflammatory response secondary to degeneration of LC
508 projections.
509 Historically, the LC has been implicated in arousal state and stress responses. For
510 example, LC activity tracks with sleep cycles (with highest firing during wake and
511 immediately preceding sleep-wake transitions), and chemogenetic or optogenetic
512 activation of LC neurons increases wakefulness (Carter et al., 2010; Vazey and Aston-
513 Jones, 2014; Porter-Stransky et al., 2019). Furthermore, the LC is activated by stress,
514 and stimulation of LC neurons elicits anxiety-like behaviors (Valentino and Van
515 Bockstaele, 2008; McCall et al., 2015). DBH-hSNCA mice exhibited age-dependent
516 behavioral phenotypes that peaked at 14-mos and are consistent with LC hyperactivity
517 and increased NE transmission. Specifically, compared to nTg littermates, DBH-hSNCA
518 mice displayed increased arousal (as measured by latency to fall asleep), anxiety (as
519 measured by marble burying and latency to re-enter the center of an open field), and
520 stress responses (as measured by freezing during fear conditioning training and context
521 re-exposure). These phenotypes are relevant to multiple non-motor symptoms of PD.
522 Sleep disturbances are one of the most common complaints of PD patients, and patients
523 who experience disturbed sleep appear to have greater LC asyn pathology than those
524 who do not report sleep disturbances (Kalaitzakis et al., 2013). Anxiety is also a common
525 complaint, as up to 60% of PD patients report experiencing anxiety (Chaudhuri and
526 Schapira, 2009; Lin et al., 2015). Importantly, DBH-hSNCA mice did not display changes
527 in the number or speed of ambulations relative to nTg mice at any age examined, ruling
528 out a general locomotor abnormality that has been observed in more ubiquitous asyn

529 overexpression mice (Giasson et al., 2002; Fleming et al., 2004; Graham and Sidhu,
530 2010).
531 We have previously speculated that asyn pathology promotes LC hyperactivity and non-
532 motor symptoms during PD progression prior to the degeneration of noradrenergic
533 neurons later in the disease (Weinshenker, 2018), and the present data support that idea.
534 Indeed, the behavioral phenotypes we observed were most prominent at 14-mos, while
535 degeneration of LC fibers was not evident until 24-mos, a time when behavioral
536 abnormalities abated. There are several potential mechanisms by which increases in
537 asyn may be affecting the LC-NE system (Fig 13). TH protein was increased in 3- and
538 14-mo old Tg mice, which is when behavioral phenotypes consistent with NE over-activity
539 emerged. Because TH is the rate-limiting enzyme in NE production, this may reflect
540 increased NE synthetic capacity, although the relevance is not clear because we did not
541 detect differences in tissue NE content. Human wild-type asyn has been reported to
542 increase in the size, and delay in the closing, of the vesicular fusion pore, allowing more
543 neurotransmitter to spill into the extracellular space (Larsen et al., 2006; Logan et al.,
544 2017). In addition, viral-mediated overexpression of A53T mutant asyn in LC neurons
545 causes increased firing rate (Henrich et al., 2018). Alternatively, if human asyn expression
546 is negatively impacting LC neuron health as suggested by the presence of asyn
547 aggregates at 14-mos and the loss of hippocampal LC fibers at 24-mos, there may be
548 compensatory increases in neuronal activity. Chemical lesion of LC neurons transiently
549 increases NE neurotransmission by increasing neuronal firing frequency and activity
550 patterns (Szot et al., 2016). Future studies directly examining LC neuron firing and NE
551 release will be necessary to identify the mechanism in play here.

552 Little is known about the potential involvement of other brainstem NE regions in PD. One
553 study reported increased DBH activity in the A2/C2 of PD patients versus healthy controls
554 (Molinoff and Axelrod, 1971; Kopp et al., 1982). While generally considered an integrative
555 region for autonomic functions, A2/C2 neurons are activated by stress and can influence
556 behavior (Cecchi et al., 2002; Ritter et al., 2003). Future studies are required to determine
557 if other central noradrenergic regions contribute to the DBH-hSNCA phenotype.
558 LC neurons are among the first affected in PD, and the features of DBH-hSNCA mice
559 may represent early pathology and non-motor components of PD that provide insight into
560 the functional impact of human asyn expression in LC neurons during aging. Additionally,
561 studies involving exposure to environmental factors that synergize with asyn expression
562 to influence the risk of PD will likely elucidate the genetic and environmental interactions
563 that contribute to LC involvement in the pre-clinical pre-motor stages of PD, as well as
564 the impact of LC degeneration on the trajectory of PD pathogenesis.
565

566 **References**

567

568 Abbott RD, Ross GW, White LR, Tanner CM, Masaki KH, Nelson JS, Curb JD, Petrovitch H (2005)
569 Excessive daytime sleepiness and subsequent development of Parkinson disease.
570 Neurology 65:1442-1446.
571 Baekelandt V, Claeys A, Eggermont K, Lauwers E, De Strooper B, Nuttin B, Debyser Z (2002)
572 Characterization of lentiviral vector-mediated gene transfer in adult mouse brain. Hum
573 Gene Ther 13:841-853.
574 Bharani KL, Derex R, Granholm AC, Ledreux A (2017) A noradrenergic lesion aggravates the
575 effects of systemic inflammation on the hippocampus of aged rats. PLoS One
576 12:e0189821.
577 Braak E, Sandmann-Keil D, Rub U, Gai WP, de Vos RA, Steur EN, Arai K, Braak H (2001) alpha-
578 synuclein immunopositive Parkinson's disease-related inclusion bodies in lower brain
579 stem nuclei. Acta Neuropathol 101:195-201.
580 Britton DR, Britton KT (1981) A sensitive open field measure of anxiolytic drug activity.
581 Pharmacol Biochem Behav 15:577-582.
582 Brunnstrom H, Friberg N, Lindberg E, Englund E (2011) Differential degeneration of the locus
583 coeruleus in dementia subtypes. Clin Neuropathol 30:104-110.
584 Butkovich LM, Houser MC, Tansey MG (2018) alpha-Synuclein and Noradrenergic Modulation of
585 Immune Cells in Parkinson's Disease Pathogenesis. Front Neurosci 12:626.
586 Carter ME, Yizhar O, Chikahisa S, Nguyen H, Adamantidis A, Nishino S, Deisseroth K, de Lecea L
587 (2010) Tuning arousal with optogenetic modulation of locus coeruleus neurons. Nat
588 Neurosci 13:1526-1533.
589 Cecchi M, Khoshbouei H, Javors M, Morilak DA (2002) Modulatory effects of norepinephrine in
590 the lateral bed nucleus of the stria terminalis on behavioral and neuroendocrine
591 responses to acute stress. Neuroscience 112:13-21.
592 Chalermpalanupap T, Schroeder JP, Rorabaugh JM, Liles LC, Lah JJ, Levey AI, Weinshenker D
593 (2018) Locus Coeruleus Ablation Exacerbates Cognitive Deficits, Neuropathology, and
594 Lethality in P301S Tau Transgenic Mice. J Neurosci 38:74-92.
595 Chartier-Harlin MC, Kachergus J, Roumier C, Mouroux V, Douay X, Lincoln S, Levecque C, Larvor
596 L, Andrieux J, Hulihan M, Waucquier N, Defebvre L, Amouyel P, Farrer M, Destee A
597 (2004) Alpha-synuclein locus duplication as a cause of familial Parkinson's disease.
598 Lancet 364:1167-1169.
599 Chaudhuri KR, Schapira AH (2009) Non-motor symptoms of Parkinson's disease: dopaminergic
600 pathophysiology and treatment. Lancet Neurol 8:464-474.
601 Chen X, Huddleston DE, Langley J, Ahn S, Barnum CJ, Factor SA, Levey AI, Hu X (2014)
602 Simultaneous imaging of locus coeruleus and substantia nigra with a quantitative
603 neuromelanin MRI approach. Magn Reson Imaging 32:1301-1306.
604 Chevalier-Larsen E, Holzbaur EL (2006) Axonal transport and neurodegenerative disease.
605 Biochim Biophys Acta 1762:1094-1108.
606 Chu Y, Morfini GA, Langhamer LB, He Y, Brady ST, Kordower JH (2012) Alterations in axonal
607 transport motor proteins in sporadic and experimental Parkinson's disease. Brain
608 135:2058-2073.

609 Chui HC, Mortimer JA, Slager U, Zarow C, Bondareff W, Webster DD (1986) Pathologic
610 correlates of dementia in Parkinson's disease. Arch Neurol 43:991-995.
611 Cubells JF, Schroeder JP, Barrie ES, Manvich DF, Sadee W, Berg T, Mercer K, Stowe TA, Liles LC,
612 Squires KE, Mezher A, Curtin P, Perdomo DL, Szot P, Weinshenker D (2016) Human
613 Bacterial Artificial Chromosome (BAC) Transgenesis Fully Rescues Noradrenergic
614 Function in Dopamine beta-Hydroxylase Knockout Mice. PLoS One 11:e0154864.
615 Damier P, Hirsch EC, Zhang P, Agid Y, Javoy-Agid F (1993) Glutathione peroxidase, glial cells and
616 Parkinson's disease. Neuroscience 52:1-6.
617 de Sousa Rodrigues ME, Bekhbat M, Houser MC, Chang J, Walker DI, Jones DP, Oller do
618 Nascimento CMP, Barnum CJ, Tansey MG (2017) Chronic psychological stress and high-
619 fat high-fructose diet disrupt metabolic and inflammatory gene networks in the brain,
620 liver, and gut and promote behavioral deficits in mice. Brain Behav Immun 59:158-172.
621 Delenclos M, Faroqi AH, Yue M, Kurti A, Castanedes-Casey M, Rousseau L, Phillips V, Dickson
622 DW, Fryer JD, McLean PJ (2017) Neonatal AAV delivery of alpha-synuclein induces
623 pathology in the adult mouse brain. Acta Neuropathol Commun 5:51.
624 den Hartog JW, Bethlem J (1960) The distribution of Lewy bodies in the central and autonomic
625 nervous systems in idiopathic paralysis agitans. J Neurol Neurosurg Psychiatry 23:283-
626 290.
627 Devauges V, Sara SJ (1991) Memory retrieval enhancement by locus coeruleus stimulation:
628 evidence for mediation by beta-receptors. Behav Brain Res 43:93-97.
629 Duffy S, MacVicar BA (1995) Adrenergic calcium signaling in astrocyte networks within the
630 hippocampal slice. J Neurosci 15:5535-5550.
631 Eng LF, Ghirnikar RS (1994) GFAP and astrogliosis. Brain Pathol 4:229-237.
632 Fahrig T (1993) Receptor subtype involved and mechanism of norepinephrine-induced
633 stimulation of glutamate uptake into primary cultures of rat brain astrocytes. Glia 7:212-
634 218.
635 Fearnley JM, Lees AJ (1991) Ageing and Parkinson's disease: substantia nigra regional
636 selectivity. Brain 114 (Pt 5):2283-2301.
637 Ferese R, Modugno N, Campopiano R, Santilli M, Zampatti S, Giardina E, Nardone A, Postorivo
638 D, Fornai F, Novelli G, Romoli E, Ruggieri S, Gambardella S (2015) Four Copies of SNCA
639 Responsible for Autosomal Dominant Parkinson's Disease in Two Italian Siblings.
640 Parkinsons Dis 2015:546462.
641 Fleming SM, Salcedo J, Fernagut PO, Rockenstein E, Masliah E, Levine MS, Chesselet MF (2004)
642 Early and progressive sensorimotor anomalies in mice overexpressing wild-type human
643 alpha-synuclein. J Neurosci 24:9434-9440.
644 Fujita H, Tanaka J, Maeda N, Sakanaka M (1998) Adrenergic agonists suppress the proliferation
645 of microglia through beta 2-adrenergic receptor. Neurosci Lett 242:37-40.
646 Fujiwara H, Hasegawa M, Dohmae N, Kawashima A, Masliah E, Goldberg MS, Shen J, Takio K,
647 Iwatsubo T (2002) alpha-Synuclein is phosphorylated in synucleinopathy lesions. Nat Cell
648 Biol 4:160-164.
649 Gerhard A, Pavese N, Hotton G, Turkheimer F, Es M, Hammers A, Eggert K, Oertel W, Banati RB,
650 Brooks DJ (2006) In vivo imaging of microglial activation with [11C](R)-PK11195 PET in
651 idiopathic Parkinson's disease. Neurobiol Dis 21:404-412.

652 German DC, Manaye KF, White CL, 3rd, Woodward DJ, McIntire DD, Smith WK, Kalaria RN,
653 Mann DM (1992) Disease-specific patterns of locus coeruleus cell loss. Ann Neurol
654 32:667-676.
655 Giasson BI, Duda JE, Quinn SM, Zhang B, Trojanowski JQ, Lee VM (2002) Neuronal alpha-
656 synucleinopathy with severe movement disorder in mice expressing A53T human alpha-
657 synuclein. Neuron 34:521-533.
658 Gonera EG, van't Hof M, Berger HJ, van Weel C, Horstink MW (1997) Symptoms and duration of
659 the prodromal phase in Parkinson's disease. Mov Disord 12:871-876.
660 Graham DR, Sidhu A (2010) Mice expressing the A53T mutant form of human alpha-synuclein
661 exhibit hyperactivity and reduced anxiety-like behavior. J Neurosci Res 88:1777-1783.
662 Grenhoff J, Nisell M, Ferre S, Aston-Jones G, Svensson TH (1993) Noradrenergic modulation of
663 midbrain dopamine cell firing elicited by stimulation of the locus coeruleus in the rat. J
664 Neural Transm Gen Sect 93:11-25.
665 Gyoneva S, Traynelis SF (2013) Norepinephrine modulates the motility of resting and activated
666 microglia via different adrenergic receptors. J Biol Chem 288:15291-15302.
667 Halliday GM, Li YW, Blumbergs PC, Joh TH, Cotton RG, Howe PR, Blessing WW, Geffen LB (1990)
668 Neuropathology of immunohistochemically identified brainstem neurons in Parkinson's
669 disease. Ann Neurol 27:373-385.
670 Hansen C, Bjorklund T, Petit GH, Lundblad M, Murmu RP, Brundin P, Li JY (2013) A novel alpha-
671 synuclein-GFP mouse model displays progressive motor impairment, olfactory
672 dysfunction and accumulation of alpha-synuclein-GFP. Neurobiol Dis 56:145-155.
673 Haycock JW (1993) Multiple signaling pathways in bovine chromaffin cells regulate tyrosine
674 hydroxylase phosphorylation at Ser19, Ser31, and Ser40. Neurochem Res 18:15-26.
675 Heneka MT, Nadrigny F, Regen T, Martinez-Hernandez A, Dumitrescu-Ozimek L, Terwel D,
676 Jardanhazi-Kurutz D, Walter J, Kirchhoff F, Hanisch UK, Kummer MP (2010) Locus
677 ceruleus controls Alzheimer's disease pathology by modulating microglial functions
678 through norepinephrine. Proc Natl Acad Sci U S A 107:6058-6063.
679 Henrich MT, Geibl FF, Lee B, Chiu WH, Koprich JB, Brotchie JM, Timmermann L, Decher N,
680 Matschke LA, Oertel WH (2018) A53T-alpha-synuclein overexpression in murine locus
681 coeruleus induces Parkinson's disease-like pathology in neurons and glia. Acta
682 Neuropathol Commun 6:39.
683 Hirsch E, Graybiel AM, Agid YA (1988) Melanized dopaminergic neurons are differentially
684 susceptible to degeneration in Parkinson's disease. Nature 334:345-348.
685 Hobson JA, McCarley RW, Wyzinski PW (1975) Sleep cycle oscillation: reciprocal discharge by
686 two brainstem neuronal groups. Science 189:55-58.
687 Hornykiewicz O (1998) Biochemical aspects of Parkinson's disease. Neurology 51:S2-9.
688 Hunsley MS, Palmiter RD (2004) Altered sleep latency and arousal regulation in mice lacking
689 norepinephrine. Pharmacol Biochem Behav 78:765-773.
690 Ip CW, Klaus LC, Karikari AA, Visanji NP, Brotchie JM, Lang AE, Volkmann J, Koprich JB (2017)
691 AAV1/2-induced overexpression of A53T-alpha-synuclein in the substantia nigra results
692 in degeneration of the nigrostriatal system with Lewy-like pathology and motor
693 impairment: a new mouse model for Parkinson's disease. Acta Neuropathol Commun
694 5:11.

695 Iversen LL, Rossor MN, Reynolds GP, Hills R, Roth M, Mountjoy CQ, Foote SL, Morrison JH,
696 Bloom FE (1983) Loss of pigmented dopamine-beta-hydroxylase positive cells from locus
697 coeruleus in senile dementia of Alzheimer's type. Neurosci Lett 39:95-100.
698 Johnson JD, Zimomra ZR, Stewart LT (2013) Beta-adrenergic receptor activation primes
699 microglia cytokine production. J Neuroimmunol 254:161-164.
700 Kalaitzakis ME, Gentleman SM, Pearce RK (2013) Disturbed sleep in Parkinson's disease:
701 anatomical and pathological correlates. Neuropathol Appl Neurobiol 39:644-653.
702 Keren NI, Taheri S, Vazey EM, Morgan PS, Granholm AC, Aston-Jones GS, Eckert MA (2015)
703 Histologic validation of locus coeruleus MRI contrast in post-mortem tissue. Neuroimage
704 113:235-245.
705 Kilbourn MR, Sherman P, Abbott LC (1998) Reduced MPTP neurotoxicity in striatum of the
706 mutant mouse tottering. Synapse 30:205-210.
707 Kim YS, Joh TH (2006) Microglia, major player in the brain inflammation: their roles in the
708 pathogenesis of Parkinson's disease. Exp Mol Med 38:333-347.
709 Kirik D, Rosenblad C, Burger C, Lundberg C, Johansen TE, Muzyczka N, Mandel RJ, Bjorklund A
710 (2002) Parkinson-like neurodegeneration induced by targeted overexpression of alpha-
711 synuclein in the nigrostriatal system. J Neurosci 22:2780-2791.
712 Kopp N, Denoroy L, Tommasi M, Gay N, Chazot G, Renaud B (1982) Increase in noradrenaline-
713 synthesizing enzyme activity in medulla oblongata in Parkinson's disease. Acta
714 Neuropathol 56:17-21.
715 Koprich JB, Johnston TH, Reyes MG, Sun X, Brotchie JM (2010) Expression of human A53T alpha-
716 synuclein in the rat substantia nigra using a novel AAV1/2 vector produces a rapidly
717 evolving pathology with protein aggregation, dystrophic neurite architecture and
718 nigrostriatal degeneration with potential to model the pathology of Parkinson's disease.
719 Mol Neurodegener 5:43.
720 Kreiner G, Rafa-Zablocka K, Barut J, Chmielarz P, Kot M, Baginska M, Parlato R, Daniel WA,
721 Nalepa I (2019) Stimulation of noradrenergic transmission by reboxetine is beneficial for
722 a mouse model of progressive parkinsonism. Sci Rep 9:5262.
723 Kumer SC, Vrana KE (1996) Intricate regulation of tyrosine hydroxylase activity and gene
724 expression. J Neurochem 67:443-462.
725 Larsen KE, Schmitz Y, Troyer MD, Mosharov E, Dietrich P, Quazi AZ, Savalle M, Nemani V,
726 Chaudhry FA, Edwards RH, Stefanis L, Sulzer D (2006) Alpha-synuclein overexpression in
727 PC12 and chromaffin cells impairs catecholamine release by interfering with a late step
728 in exocytosis. J Neurosci 26:11915-11922.
729 Lategan AJ, Marien MR, Colpaert FC (1990) Effects of locus coeruleus lesions on the release of
730 endogenous dopamine in the rat nucleus accumbens and caudate nucleus as
731 determined by intracerebral microdialysis. Brain Res 523:134-138.
732 Leenders KL, Salmon EP, Tyrrell P, Perani D, Brooks DJ, Sager H, Jones T, Marsden CD,
733 Frackowiak RS (1990) The nigrostriatal dopaminergic system assessed in vivo by positron
734 emission tomography in healthy volunteer subjects and patients with Parkinson's
735 disease. Arch Neurol 47:1290-1298.
736 Levitt M, Spector S, Sjoerdsma A, Udenfriend S (1965) Elucidation of the Rate-Limiting Step in
737 Norepinephrine Biosynthesis in the Perfused Guinea-Pig Heart. J Pharmacol Exp Ther
738 148:1-8.

739 Lin CH, Lin JW, Liu YC, Chang CH, Wu RM (2015) Risk of Parkinson's disease following anxiety
740 disorders: a nationwide population-based cohort study. Eur J Neurol 22:1280-1287.
741 Logan T, Bendor J, Toupin C, Thorn K, Edwards RH (2017) alpha-Synuclein promotes dilation of
742 the exocytotic fusion pore. Nat Neurosci 20:681-689.
743 Mann JJ, Stanley M, Kaplan RD, Sweeney J, Neophytides A (1983) Central catecholamine
744 metabolism in vivo and the cognitive and motor deficits in Parkinson's disease. J Neurol
745 Neurosurg Psychiatry 46:905-910.
746 Maskri L, Zhu X, Fritzen S, Kuhn K, Ullmer C, Engels P, Andriske M, Stichel CC, Lubbert H (2004)
747 Influence of different promoters on the expression pattern of mutated human alpha-
748 synuclein in transgenic mice. Neurodegener Dis 1:255-265.
749 Masliah E, Rockenstein E, Veinbergs I, Mallory M, Hashimoto M, Takeda A, Sagara Y, Sisk A,
750 Mucke L (2000) Dopaminergic loss and inclusion body formation in alpha-synuclein
751 mice: implications for neurodegenerative disorders. Science 287:1265-1269.
752 Mavridis M, Degryse AD, Lategan AJ, Marien MR, Colpaert FC (1991) Effects of locus coeruleus
753 lesions on parkinsonian signs, striatal dopamine and substantia nigra cell loss after 1-
754 methyl-4-phenyl-1,2,3,6-tetrahydropyridine in monkeys: a possible role for the locus
755 coeruleus in the progression of Parkinson's disease. Neuroscience 41:507-523.
756 McCall JG, Al-Hasani R, Siuda ER, Hong DY, Norris AJ, Ford CP, Bruchas MR (2015) CRH
757 Engagement of the Locus Coeruleus Noradrenergic System Mediates Stress-Induced
758 Anxiety. Neuron 87:605-620.
759 McGeer PL, Itagaki S, Boyes BE, McGeer EG (1988) Reactive microglia are positive for HLA-DR in
760 the substantia nigra of Parkinson's and Alzheimer's disease brains. Neurology 38:1285-
761 1291.
762 Molinoff PB, Axelrod J (1971) Biochemistry of catecholamines. Annu Rev Biochem 40:465-500.
763 Murchison CF, Zhang XY, Zhang WP, Ouyang M, Lee A, Thomas SA (2004) A distinct role for
764 norepinephrine in memory retrieval. Cell 117:131-143.
765 Niu H, Shen L, Li T, Ren C, Ding S, Wang L, Zhang Z, Liu X, Zhang Q, Geng D, Wu X, Li H (2018)
766 Alpha-synuclein overexpression in the olfactory bulb initiates prodromal symptoms and
767 pathology of Parkinson's disease. Transl Neurodegener 7:25.
768 Norris JG, Benveniste EN (1993) Interleukin-6 production by astrocytes: induction by the
769 neurotransmitter norepinephrine. J Neuroimmunol 45:137-145.
770 Paukert M, Agarwal A, Cha J, Doze VA, Kang JU, Bergles DE (2014) Norepinephrine controls
771 astroglial responsiveness to local circuit activity. Neuron 82:1263-1270.
772 Pavese N, Rivero-Bosch M, Lewis SJ, Whone AL, Brooks DJ (2011) Progression of monoaminergic
773 dysfunction in Parkinson's disease: a longitudinal 18F-dopa PET study. Neuroimage
774 56:1463-1468.
775 Phillips RG, LeDoux JE (1992) Differential contribution of amygdala and hippocampus to cued
776 and contextual fear conditioning. Behav Neurosci 106:274-285.
777 Pifl C, Kish SJ, Hornykiewicz O (2012) Thalamic noradrenaline in Parkinson's disease: deficits
778 suggest role in motor and non-motor symptoms. Mov Disord 27:1618-1624.
779 Porter-Stransky KA, Centanni SW, Karne SL, Odil LM, Fekir S, Wong JC, Jerome C, Mitchell HA,
780 Escayg A, Pedersen NP, Winder DG, Mitrano DA, Weinshenker D (2019) Noradrenergic
781 Transmission at Alpha1-Adrenergic Receptors in the Ventral Periaqueductal Gray
782 Modulates Arousal. Biol Psychiatry 85:237-247.

783 Remy P, Doder M, Lees A, Turjanski N, Brooks D (2005) Depression in Parkinson's disease: loss
784 of dopamine and noradrenaline innervation in the limbic system. Brain 128:1314-1322.
785 Ritter S, Watts AG, Dinh TT, Sanchez-Watts G, Pedrow C (2003) Immunotoxin lesion of
786 hypothalamically projecting norepinephrine and epinephrine neurons differentially
787 affects circadian and stressor-stimulated corticosterone secretion. Endocrinology
788 144:1357-1367.
789 Rommelfanger KS, Weinshenker D (2007) Norepinephrine: The redheaded stepchild of
790 Parkinson's disease. Biochem Pharmacol 74:177-190.
791 Rommelfanger KS, Weinshenker D, Miller GW (2004) Reduced MPTP toxicity in noradrenaline
792 transporter knockout mice. J Neurochem 91:1116-1124.
793 Rommelfanger KS, Edwards GL, Freeman KG, Liles LC, Miller GW, Weinshenker D (2007)
794 Norepinephrine loss produces more profound motor deficits than MPTP treatment in
795 mice. Proc Natl Acad Sci U S A 104:13804-13809.
796 Rorabaugh JM, Chalermpalanupap T, Botz-Zapp CA, Fu VM, Lembeck NA, Cohen RM,
797 Weinshenker D (2017) Chemogenetic locus coeruleus activation restores reversal
798 learning in a rat model of Alzheimer's disease. Brain 140:3023-3038.
799 Ross GW, Petrovitch H, Abbott RD, Tanner CM, Popper J, Masaki K, Launer L, White LR (2008)
800 Association of olfactory dysfunction with risk for future Parkinson's disease. Ann Neurol
801 63:167-173.
802 Sawamoto K, Nakao N, Kobayashi K, Matsushita N, Takahashi H, Kakishita K, Yamamoto A,
803 Yoshizaki T, Terashima T, Murakami F, Itakura T, Okano H (2001) Visualization, direct
804 isolation, and transplantation of midbrain dopaminergic neurons. Proc Natl Acad Sci U S
805 A 98:6423-6428.
806 Schank JR, Ventura R, Puglisi-Allegra S, Alcaro A, Cole CD, Liles LC, Seeman P, Weinshenker D
807 (2006) Dopamine beta-hydroxylase knockout mice have alterations in dopamine
808 signaling and are hypersensitive to cocaine. Neuropsychopharmacology 31:2221-2230.
809 Schell H, Hasegawa T, Neumann M, Kahle PJ (2009) Nuclear and neuritic distribution of serine-
810 129 phosphorylated alpha-synuclein in transgenic mice. Neuroscience 160:796-804.
811 Singleton AB et al. (2003) alpha-Synuclein locus triplication causes Parkinson's disease. Science
812 302:841.
813 Song CH, Fan X, Exeter CJ, Hess EJ, Jinnah HA (2012) Functional analysis of dopaminergic
814 systems in a DYT1 knock-in mouse model of dystonia. Neurobiol Dis 48:66-78.
815 Song S, Jiang L, Oyarzabal EA, Wilson B, Li Z, Shih YI, Wang Q, Hong JS (2018) Loss of Brain
816 Norepinephrine Elicits Neuroinflammation-Mediated Oxidative Injury and Selective
817 Caudo-Rostral Neurodegeneration. Mol Neurobiol.
818 Sotiriou E, Vassilatis DK, Vila M, Stefanis L (2010) Selective noradrenergic vulnerability in alpha-
819 synuclein transgenic mice. Neurobiol Aging 31:2103-2114.
820 Spillantini MG, Schmidt ML, Lee VM, Trojanowski JQ, Jakes R, Goedert M (1997) Alpha-synuclein
821 in Lewy bodies. Nature 388:839-840.
822 Srinivasan J, Schmidt WJ (2003) Potentiation of parkinsonian symptoms by depletion of locus
823 coeruleus noradrenaline in 6-hydroxydopamine-induced partial degeneration of
824 substantia nigra in rats. Eur J Neurosci 17:2586-2592.
825 Szot P, Franklin A, Miguelez C, Wang Y, Vidaurrazaga I, Ugedo L, Sikkema C, Wilkinson CW,
826 Raskind MA (2016) Depressive-like behavior observed with a minimal loss of locus

827 coeruleus (LC) neurons following administration of 6-hydroxydopamine is associated
828 with electrophysiological changes and reversed with precursors of norepinephrine.
829 Neuropharmacology 101:76-86.
830 Tansey MG, Goldberg MS (2010) Neuroinflammation in Parkinson's disease: its role in neuronal
831 death and implications for therapeutic intervention. Neurobiol Dis 37:510-518.
832 Tong J, Hornykiewicz O, Kish SJ (2006) Inverse relationship between brain noradrenaline level
833 and dopamine loss in Parkinson disease: a possible neuroprotective role for
834 noradrenaline. Arch Neurol 63:1724-1728.
835 Valentino RJ, Van Bockstaele E (2008) Convergent regulation of locus coeruleus activity as an
836 adaptive response to stress. Eur J Pharmacol 583:194-203.
837 Vazey EM, Aston-Jones G (2014) Designer receptor manipulations reveal a role of the locus
838 coeruleus noradrenergic system in isoflurane general anesthesia. Proc Natl Acad Sci U S
839 A 111:3859-3864.
840 Wakamatsu M, Ishii A, Ukai Y, Sakagami J, Iwata S, Ono M, Matsumoto K, Nakamura A, Tada N,
841 Kobayashi K, Iwatsubo T, Yoshimoto M (2007) Accumulation of phosphorylated alpha-
842 synuclein in dopaminergic neurons of transgenic mice that express human alpha-
843 synuclein. J Neurosci Res 85:1819-1825.
844 Weinshenker D (2018) Long Road to Ruin: Noradrenergic Dysfunction in Neurodegenerative
845 Disease. Trends Neurosci 41:211-223.
846 Yao N, Wu Y, Zhou Y, Ju L, Liu Y, Ju R, Duan D, Xu Q (2015) Lesion of the locus coeruleus
847 aggravates dopaminergic neuron degeneration by modulating microglial function in
848 mouse models of Parkinsons disease. Brain Res 1625:255-274.
849 Zarow C, Lyness SA, Mortimer JA, Chui HC (2003) Neuronal loss is greater in the locus coeruleus
850 than nucleus basalis and substantia nigra in Alzheimer and Parkinson diseases. Arch
851 Neurol 60:337-341.
852
853

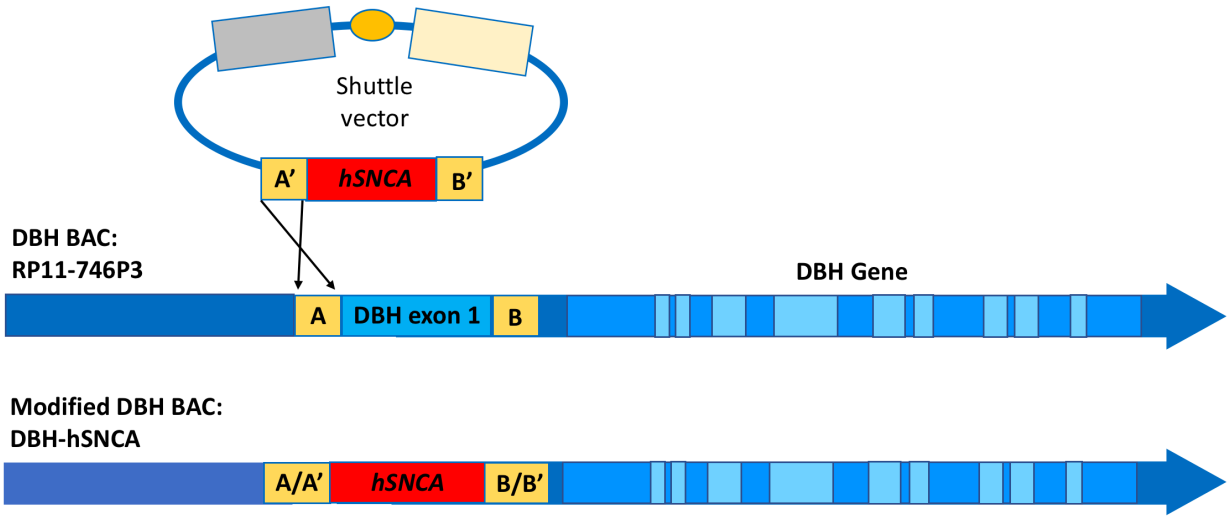

Figure 1: *hSNCA* cDNA open reading frame was targeted to the translational start site of *DBH* by standard BAC recombineering methods

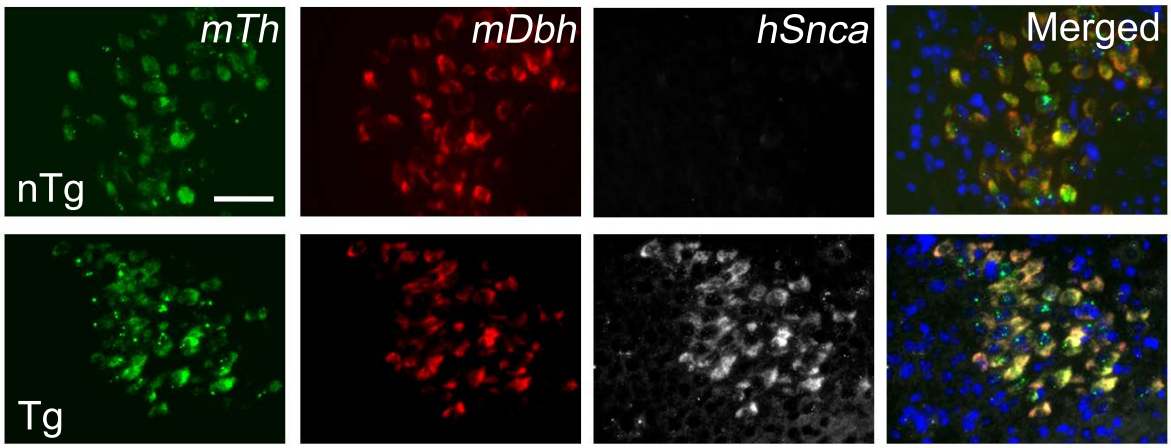

Figure 2: Human *Snca* mRNA is expressed in DBH-hSNCA locus coeruleus neurons. Human *Snca* mRNA (hSnca; white) expression is detectable only in transgenic (Tg: bottom row) LC neurons, where it co-localizes with mouse *Th* mRNA (mTh, green), and mouse *Dbh* mRNA (mDbh; red) using RNA Scope Fluorescent Multiplex v2 assay. Scale bar = 50μm.

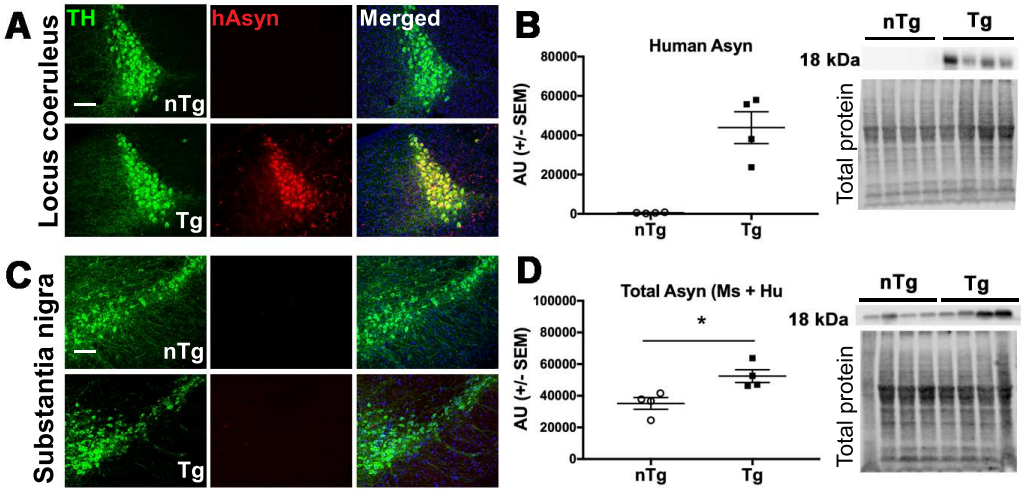

Figure 3: Analysis of asyn expression in locus coeruleus of young DBH-hSNCA mice. ***A,*** Immunofluorescent detection of human asyn (red) with a species-specific antibody (Biolegend 807801) demonstrates co-localization with TH-expressing LC neurons (green) in Tg mice (lower panel) but not in nTg mice (upper panel), or in ***C,*** TH-expressing neurons (green) in the substantia nigra regardless of genotype. ***B,*** Human asyn protein is expressed selectively in LC neurons of Tg mice by western blot. ***D,*** Immunoblot of LC protein with an antibody against asyn that detects the mouse and human protein reveals a significant increase in total asyn protein expression in Tg LC neurons as compared to that in LC of nTg littermate mice. Immunoblot data graphed as arbitrary units (AU) normalized to total protein. All data are from 3-mo old nTg and Tg mice. Scale bar = 50μm. Student's t-test ± SEM *$p<0.05$.

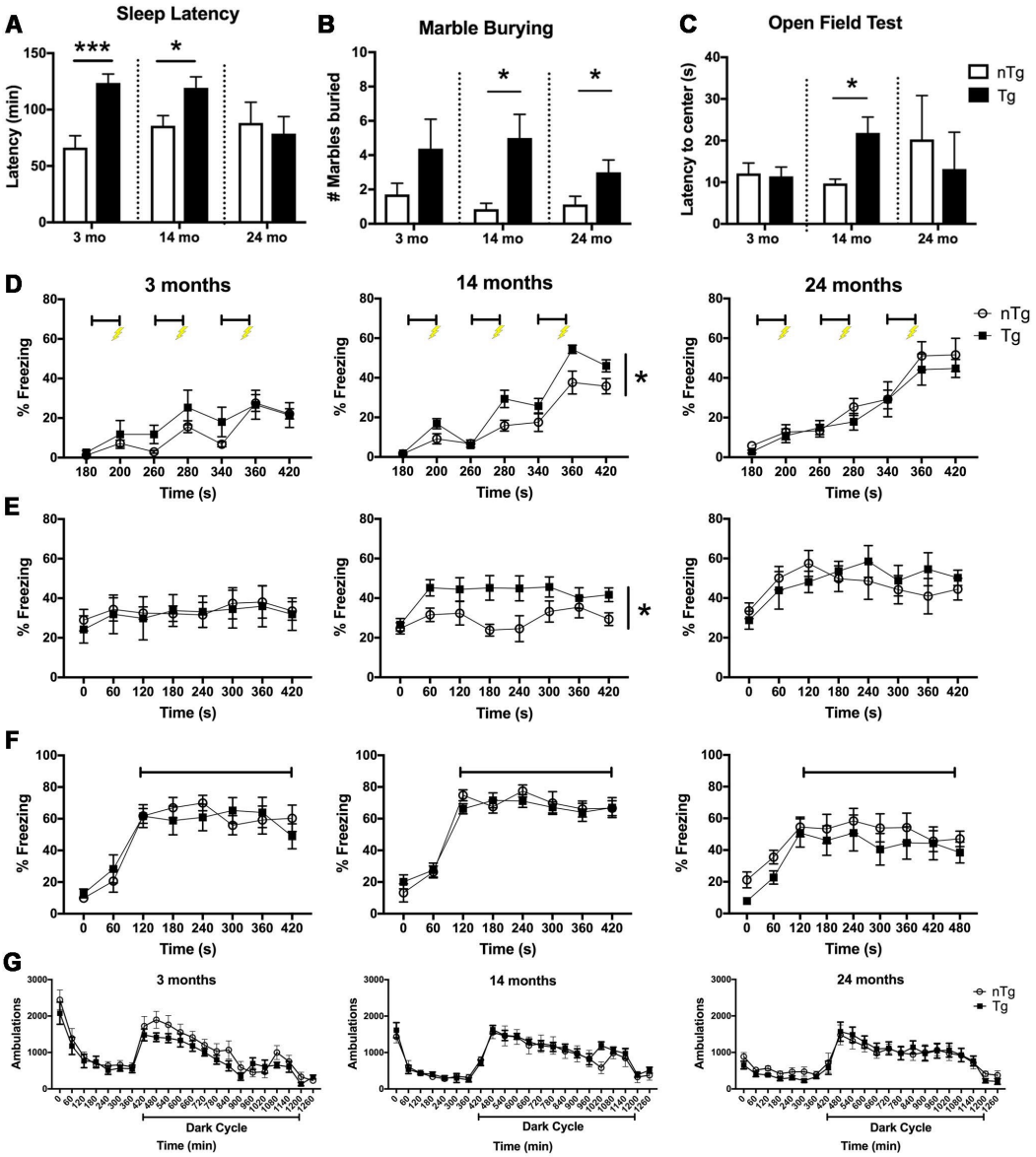

Figure 4: DBH-hSNCA mice display age-dependent behavioral abnormalities similar to the non-motor symptoms of PD. *A,* 3-mo and 14-mo Tg mice have increased sleep latency. ***B,*** Tg mice display anxiety-like behavior by marble-burying test at 14-mos and 24-mos and by ***C,*** latency to re-enter the center in the open field test at 14-mos. ***D,*** There is a significant effect of genotype at 14-mos with Tg mice exhibiting significantly more percent time freezing during fear training (center panel; bars represent tone presentation, bolt represents foot shock) and ***E,*** contextual learning**.** ***F,*** There was no effect of genotype in percent time freezing during cued test at any age. ***G,*** Ambulations do not differ by genotype at any age Students t-test of genotype ± SEM in A, B & C. Repeated measures ANOVA ± SEM in D, E, F, and G. *$p<0.05$, ***$p<0.001$.

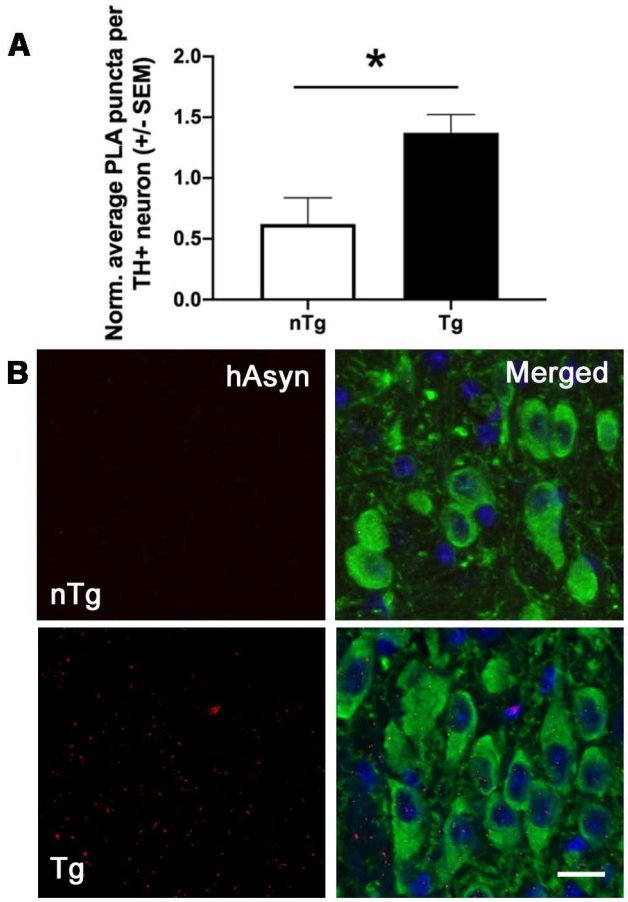

Figure 5: DBH-hSNCA LC neurons contain small asyn aggregates. *A,* At 14-mos of age, LC neurons in (TH; green) Tg mice contain significantly more oligomerized asyn (red) in LC neurons as determined by proximity ligation assay (PLA). ***B,*** Representative images. Scale bar = 15μm. Student's t-test ± SEM. *$p<0.05$.

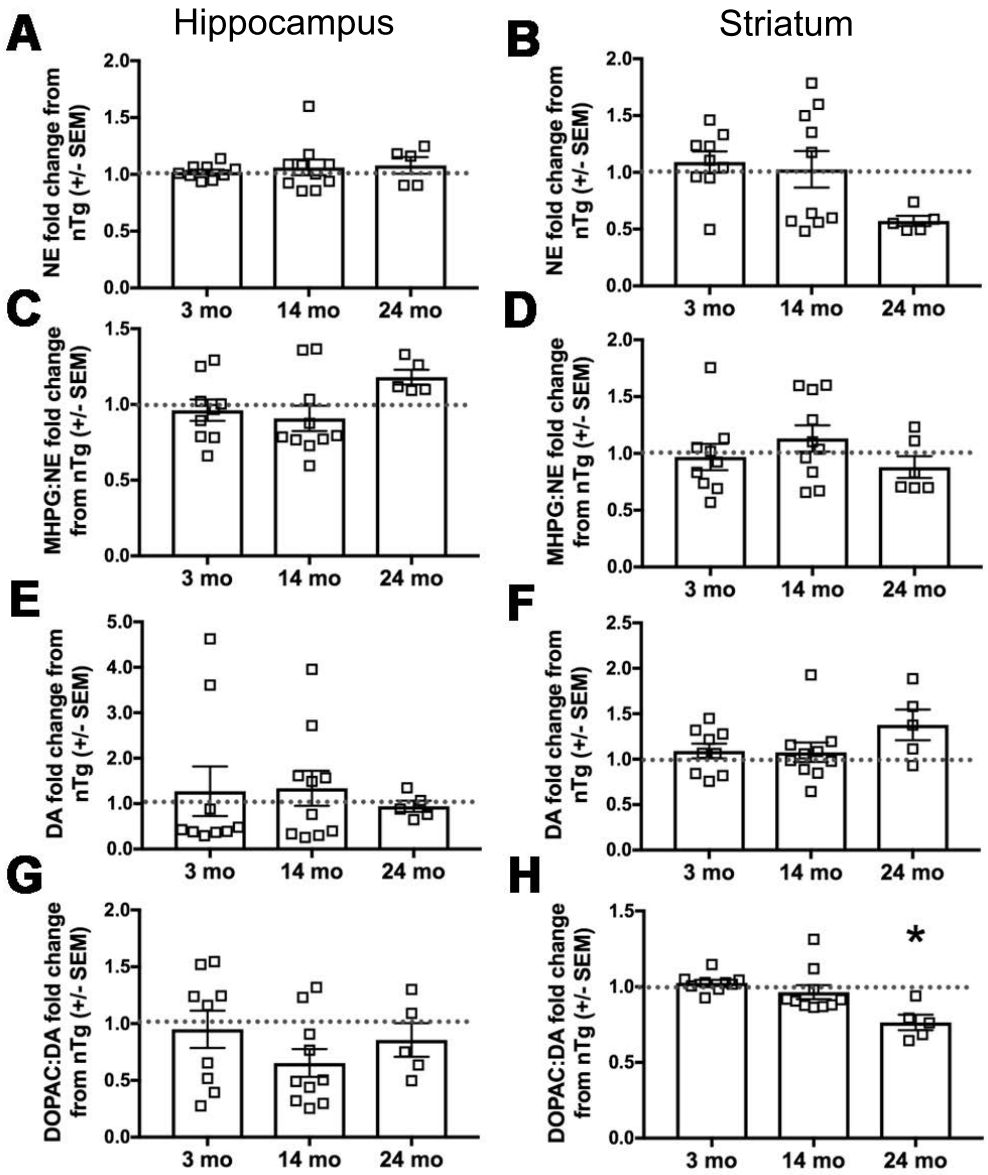

Figure 6: Human asyn expression in LC neurons impacts striatal dopamine metabolism in aged DBH-hSNCA mice. Catecholamine and catecholamine metabolite tissue content from hippocampus and striatum was measured by HPLC. ***A,*** Hippocampal NE is not affected by genotype. ***B,*** Striatal NE is reduced at 24-mos but does not reach statistical significance. The NE metabolite MHPG to NE ratio does not differ at any age in the ***C,*** hippocampus, or ***D,*** striatum. Dopamine content is not affected at any age in ***E,*** hippocampus, or ***F,*** striatum. ***G,*** The ratio of the DA metabolite DOPAC to DA is unaffected in the hippocampus ***H,*** but is significantly reduced in the striatum of Tg mice at 24-mos. Student's t-test of genotype for each age group ± SEM. *$p<0.05$.

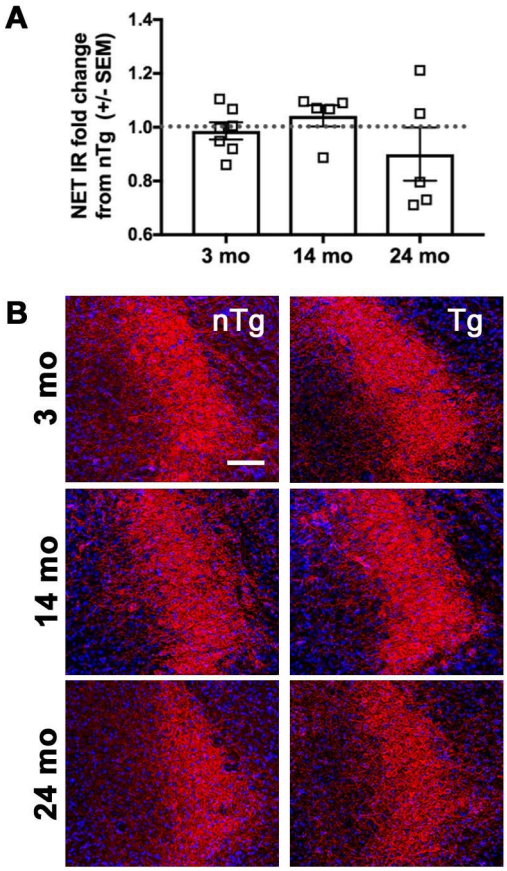

Figure 7: Human asyn expression does not affect LC integrity. NET-expressing LC cell bodies (red) percent immunoreactivity (IR) does not differ by genotype at 3-, 14-, or 24-mos. Student's t-test of mean IR by genotype for each age group, ***A,*** graphed as fold change Tg from nTg mean ± SEM. ***B,*** Representative images. Scale bar = 50µm, *$p<0.05$.

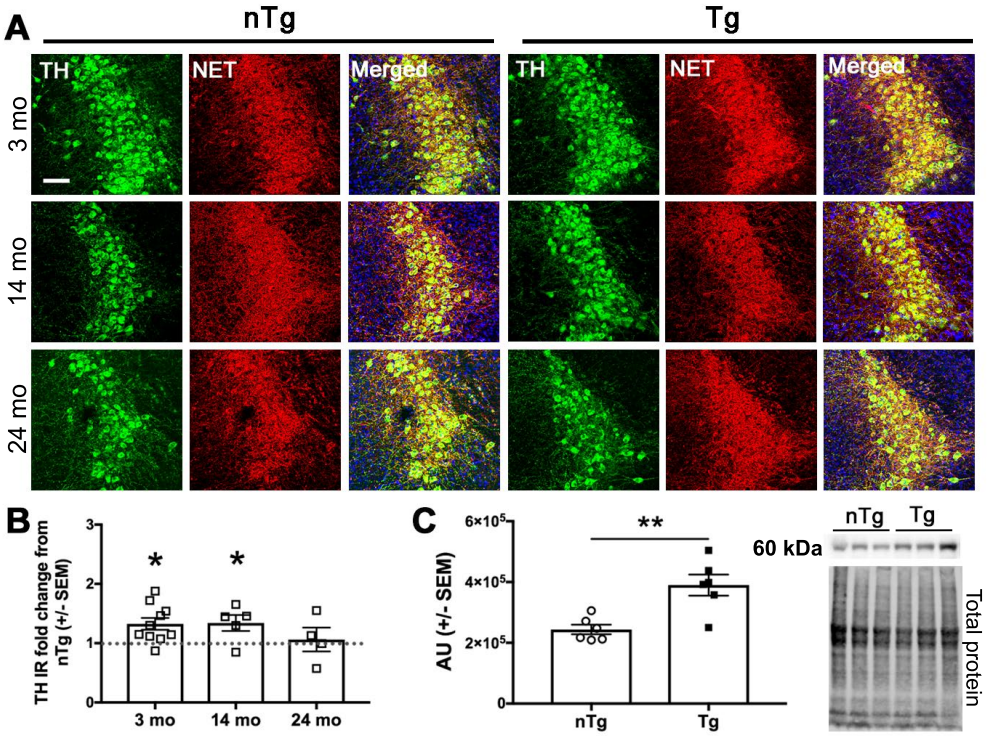

Figure 8: Tyrosine hydroxylase levels are elevated in young DBH-hSNCA Tg mice. Tyrosine hydroxylase (TH: green) immunoreactivity is increased in LC neurons (NET: red) at 3- and 14-mos of age. ***A***, Representative immunofluorescent images. ***B***, TH IR mean normalized to NET IR mean and expressed as fold change Tg from nTg mean % IR ± SEM. ***C,*** Western blot analysis of 3-mo old LC neurons confirms increased TH abundance. Data graphed as arbitrary densitometric units (AU) was normalized to total protein ± SEM. ***D,*** Representative western blot images of TH (top) and total protein stain (bottom). Student's t-test of nTg and Tg at each age, n=5-10. Scale bar = 50µm. *$p<0.05$.

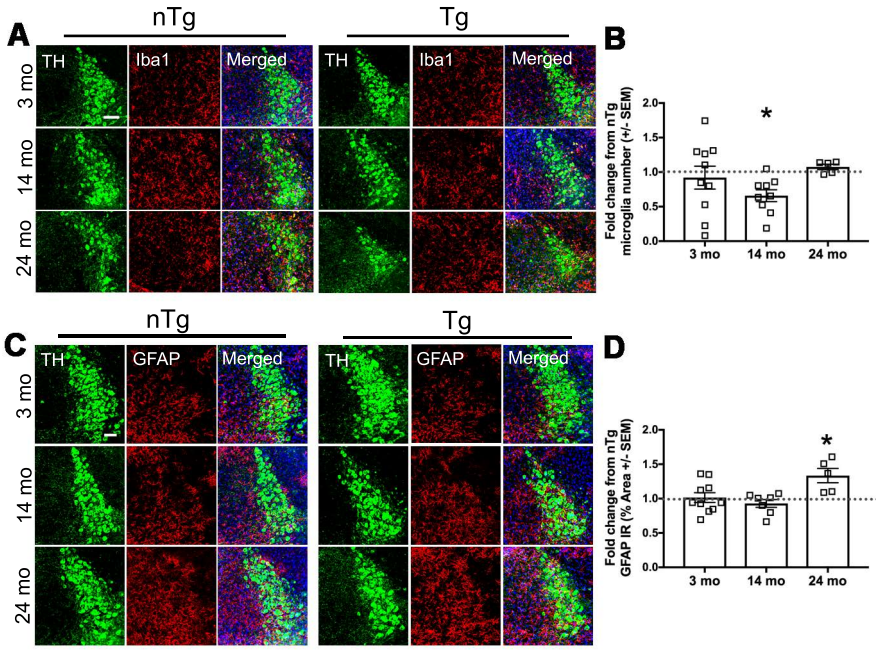

Fig 9. Human asyn in LC neurons affects expression of local inflammatory markers There are fewer Iba1-positive cells (red) in the LC (TH: green) at 14-mos. ***A***, Representative immunofluorescent images. ***B***, Microglial count in the LC graphed as fold change Tg from nTg Iba1+ cell count ± SEM. Student's t-test of nTg and Tg for each age group. Expression of astrocytic GFAP (red) is increased in the Tg LC (TH: green) at 24-mos of age. ***C***, Representative immunofluorescent images. ***D***, Quantification of GFAP % IR in the LC as percent ROI graphed as fold change Tg IR from nTg mean IR ± SEM. Student's t-test of nTg and Tg for each age group. Scale bar = 50μm. *$p<0.05$.

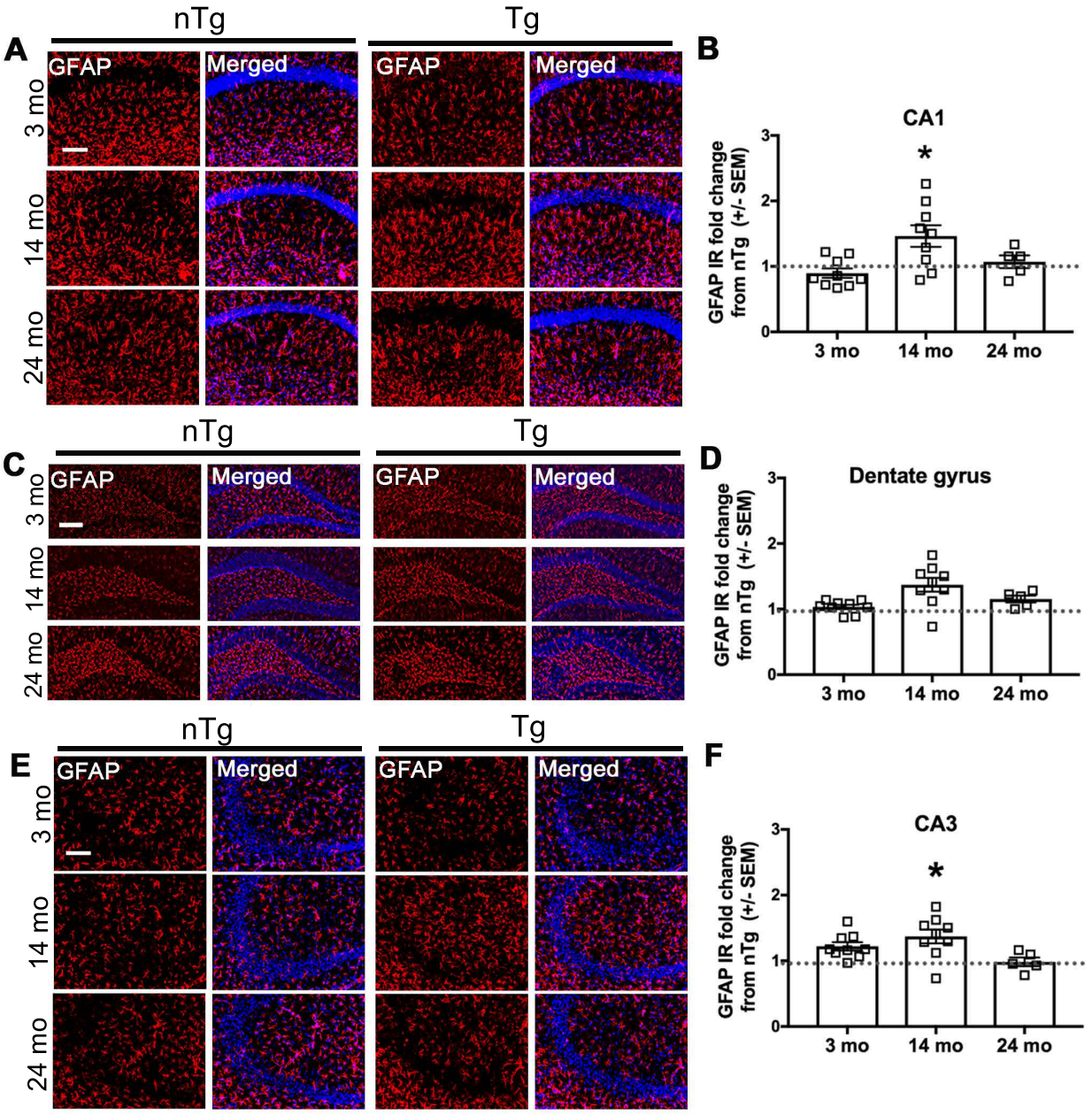

Fig 10: Hippocampal astrocytic GFAP expression is increased at 14-mos. At 14-mos, Tg mice have significantly more GFAP (red) expression than nTg in the CA1 region of the hippocampus. Representative immunofluorescent images of ***A***, CA1, ***C,*** dentate gyrus, and ***E,*** CA3 regions. Quantification of GFAP IR as % area of ROI in ***B,*** CA1, ***D,*** dentate gyrus, and ***F,*** CA3. Student's t-test of nTg and Tg for each age group, graphed as fold change Tg from nTg mean ± SEM. Scale bar = 50μm. *p<0.05.

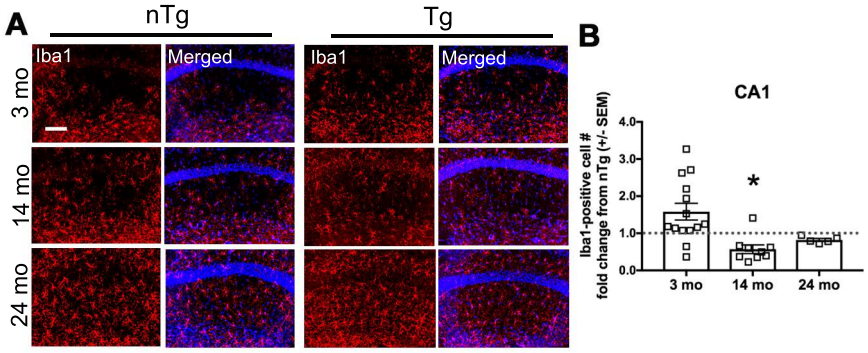

Fig 11: Fewer Iba1-expressing cells in hippocampal CA1 region in 14-mo old Tg DBH-hSNCA mice. At 14-mos, Tg mice have fewer Iba1-expressing cells in hippocampal region CA1. ***A,*** Representative immunofluorescent images of Iba1-expressing cells (red). ***B,*** Quantification of Iba1-expressing cells in CA1 graphed as Tg fold change from nTg mean ± SEM. Student's t-test by genotype for each age group. Nuclear stain in blue. Scale bar = 150μm. *$p<0.05$.

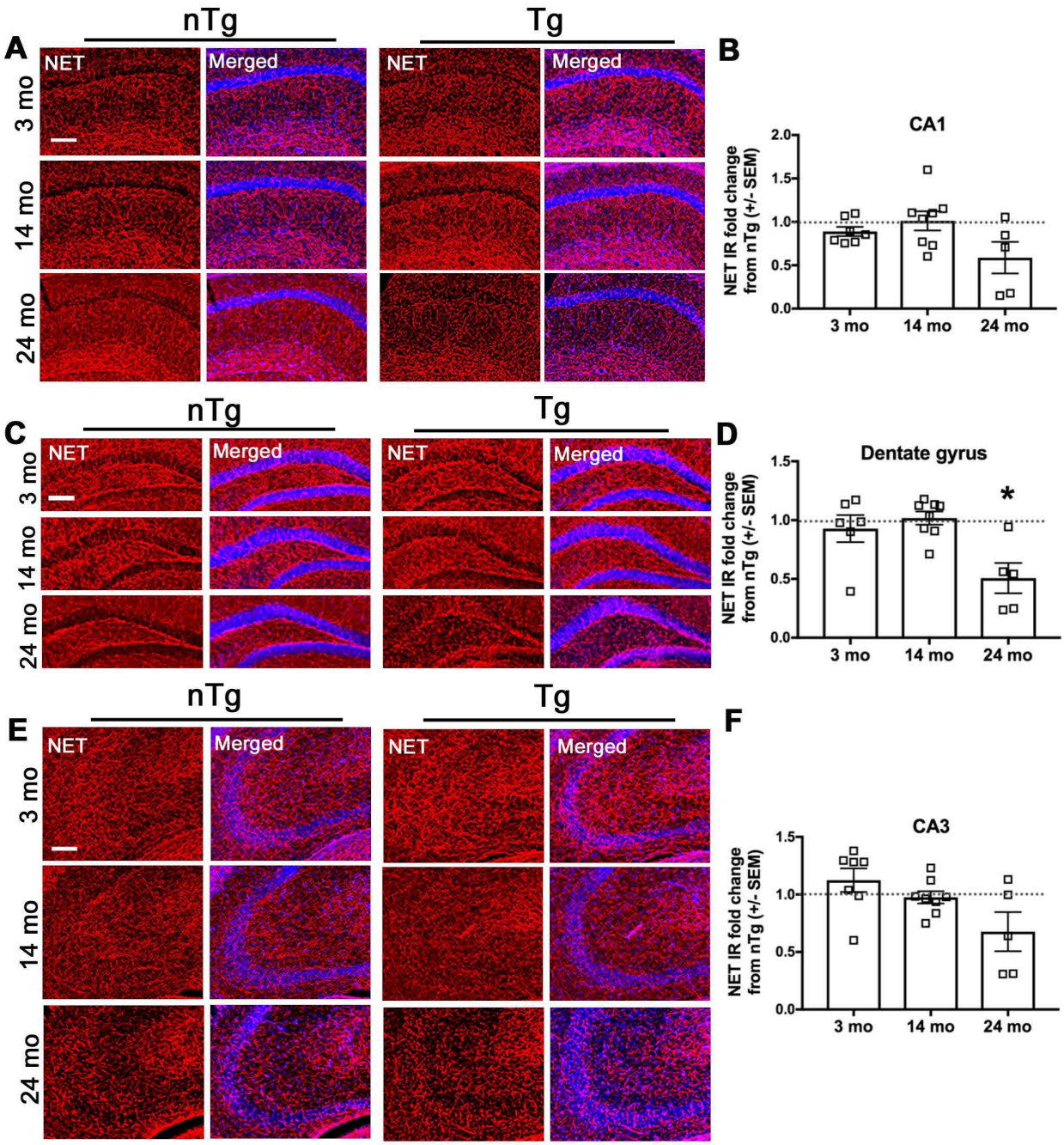

Figure 12: Asyn expression in LC neurons results in age-dependent degeneration of hippocampal LC fibers. NET (red) IR is reduced in the dentate gyrus of Tg mice at 24-mos. Representative immunofluorescent images of ***A***, CA1, ***C,*** dentate gyrus, and ***E,*** CA3 regions. Quantification of NET IR as percent area of ROI in ***B,*** CA1, ***D,*** dentate gyrus, and ***F,*** CA3. Student's t-test of nTg and Tg for each age group, graphed as fold change Tg from nTg mean ± SEM. Scale bar = 150μm. *$p<0.05$.

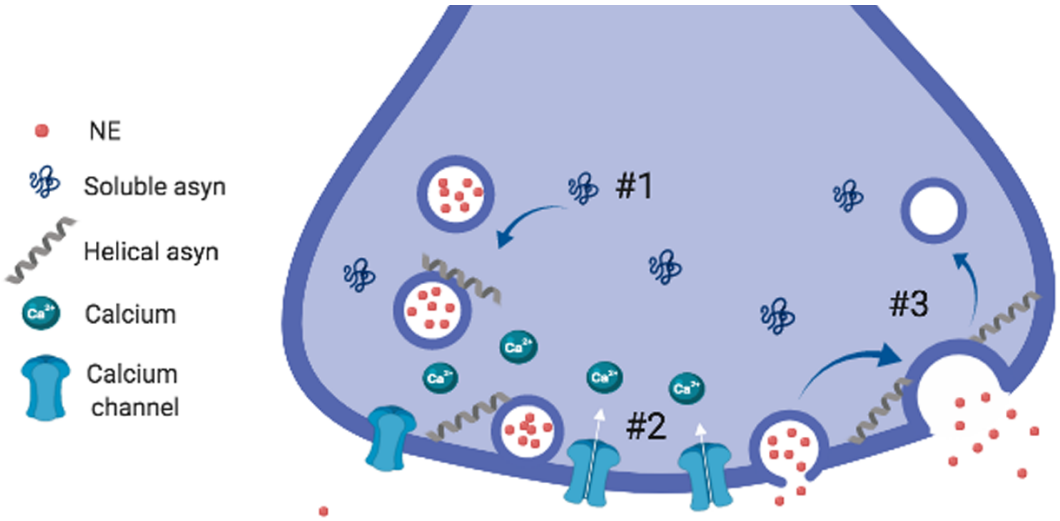

Figure 13: Asyn can directly affect neurotransmission. Asyn could enhance extracellular NE by several mechanisms. #1 – Increased expression of asyn can potentiate clustering of synaptic vesicles at the presynaptic membrane. #2 – Elevated asyn expression can reduce norepinephrine transporter (NET) expression at the plasma membrane. #3 – Asyn modulation of L-type voltage gated calcium channels can enhance neuronal excitability. #4 – Human asyn expression can enlarge the size of, and slow the closing of vesicular fusion pores, allowing more NE to spill into the extracellular space.

Table 1: Primary and secondary antibodies used in these studies

Immunofluorescence

Antigen	Host	Manufacturer	Cat. No.	Dilution
α-synuclein (Hu)	Mouse	Biolegend	807801	1:500
DAT	Rat	Millipore	MAB369	1:500
GFAP	Rabbit	Zymed	13-0300	1:500
Iba1	Rabbit	Wako	019-19741	1:500
NET	Mouse	Mab Technologies	NET05-2	1:1,000
Tyrosine hydroxylase	Rabbit	Millipore	AB152	1:1,000
Tyrosine hydroxylase	Chicken	Abcam	AB76442	1:1,000
VMAT2	Rabbit	*R.A. Cliburn et al, 2017*		1:500
Anti-chicken AlexaFluor488	Goat	Invitrogen	A11039	1:1,000
Anti-rabbit AlexaFluor488	Goat	Invitrogen	A11015	1:1,000
Anti-mouse AlexaFluor594	Goat	Invitrogen	A11020	1:1,000
Anti-rabbit AlexaFluor594	Goat	Invitrogen	A11012	1:1,000
Anti-rat AlexaFluor594	Goat	Invitrogen	A11007	1:1,000

Proximity ligation assay	Host	Manufacturer	Cat. No.	Dilution
α-synuclein (Hu)	Mouse	Abcam	AB80627	1:1000
α-synuclein- pSer129	Mouse	Biolegend	MMS-5091	1:1000
Syn-F1	Mouse	Biolegend	847802	1:1,000

Immunoblotting

Antigen	Host	Manufacturer	Cat. No.	Dilution
α-synuclein (Hu)	Mouse	Abcam	AB80627	1:1,000
α-synuclein (Ms + Hu)	Rabbit	Santa Cruz	SC-7011R	1:500
Tyrosine hydroxylase	Rabbit	Millipore	AB152	1:1,000
Anti-mouse HRP	Goat	Jackson ImmunoResearch	115-036-072	1:1,000
Anti-rabbit HRP	Goat	Jackson ImmunoResearch	111-036-047	1:1,000

1120
1121